POLITECNICO DI TORINO

MASTER OF SCIENCE IN
BIOMEDICAL ENGINEERING

DEPARTMENT OF MECHANICAL AND
AEROSPACE ENGINEERING

Microfluidic Lab-On-chip for point-of-care infectious disease diagnostics

Supervisors:
Prof. Danilo Demarchi
Dr. Pantelis Georgiou
Co-supervisor:
Dr. Jesus Rodriguez Manzano

Submitted By :
Chiara Cicatiello
(S229943)

July, 2018

The project presented in this thesis has been developed entirely at the Centre for Bio-Inspired Technology of the Imperial College London.

Contents

List of Figures

List of Tables

Acronyms

AMR antimicrobial resistance. 2

B3 backward outer primer. 11

BIP backward inner primer. 11

DEP dielectrophoresis. iii, 17, 18

DMF digital microfluidics. 15

EWOD electrowetting on dielectric. iii, 15, 18

F3 forward outer primer. 11

FIP forward inner primer. 11

ISFET Ion-Sensitive Field-Effect Transistor. iii, 19, 22

LAMP loop-mediated isothermal amplification. ii, iii, 10–12, 20, 21, 23, 25, 26, 30, 33

LoC Lab-on-Chip. 13, 20, 25, 26, 33, 47

LSI large scale integration. 18

MCU microcontroller. 21, 25

NAATs Nucleic Acid Amplification Tests. iii, 4, 12, 13

PCR polymerase chain reaction. ii, 6, 7, 9, 10, 23

PDMS polydimethylsiloxane. 14, 15, 18

POC point-of-care. 1, 10, 12, 13, 21

PTFE poly(tetrafluoroethylene). 38, 40

Real-Time PCR	real-time polymerase chain reaction. 9
SLA	stereolithography. 27
SNR	Signal-to-noise ratio. 21
WHO	World Health Organization. 1

Acknowledgements

Firstly, I would like to thank Prof. Danilo Demarchi for allowing me to take part to this incredible experience at Imperial College London. I sincerely thank Dr. Pantelis Georgiou for accepting me in his very talented research group at the Centre for Bio-Inspired Technology and providing me with the opportunity to acquire a great deal of knowledge and expertise. I also thank all students and researchers of Bio-Team with whom I had the pleasure of working during this year, especially Dr. Rodriguez Manzano for supervising and coordinating me for the entire duration of my project. Finally, I thank Mr. Rochester for help in fabricating manifolds and Dr. Karde for support in measurements.

Chapter 1

Introduction

1.1 Motivation

Over the last decade, biomedical research has heavily invested in ideas and efforts to create portable point-of-care (POC) medical diagnostic systems which could be life-changing for many people, particularly in resource-limited settings where there is no access to advanced medical diagnostic technologies.

Infectious diseases represent a significant health and economic burden, claiming millions of lives worldwide every year. According to the World Health Organization (WHO), a specialised agency of United Nations which coordinates and directs global health work, infectious diseases are still in the top 10 causes of death (see Figure 1.1). Among the communicable diseases, the lower respiratory infections remain the mainly cause of death, that caused 3 million lives in 2016. Death rate related to infectious diseases significantly decreased compared to the one in 2000, as a proof of the big success of the

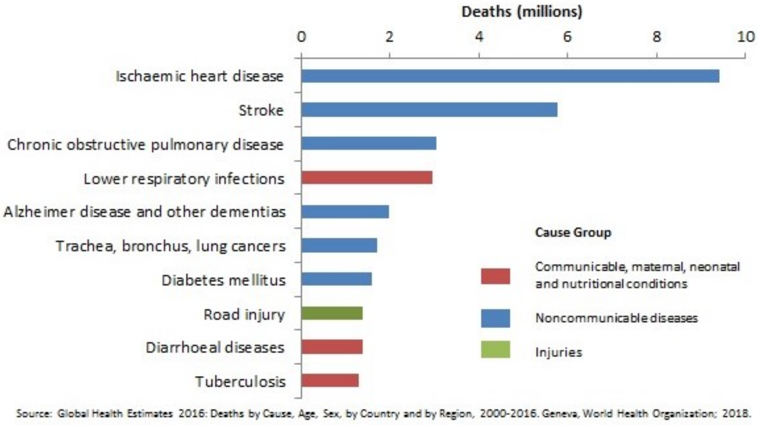

Source: Global Health Estimates 2016: Deaths by Cause, Age, Sex, by Country and by Region, 2000-2016. Geneva, World Health Organization; 2018.

Figure 1.1: Top 10 global causes of deaths, 2016 [5].

public health community in controlling infectious diseases. However, this improvement is not that evident in low-income countries, where deaths due to the “Group I” conditions, which include communicable diseases, continued to represent more than 50% of causes of death in 2016 (see Figure 1.2) [5].

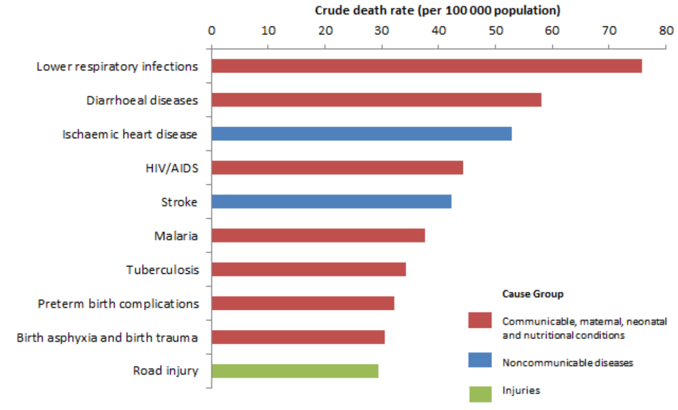

Source: Global Health Estimates 2016: Deaths by Cause, Age, Sex, by Country and by Region, 2000-2016. Geneva, World Health Organization; 2018.
World Bank list of economies (June 2017). Washington, DC: The World Bank Group; 2017 (https://datahelpdesk.worldbank.org/knowledgebase/articles/906519-world-bank-country-and-lending-groups).

Figure 1.2: Top 10 causes of deaths in low-income countries, 2016 [5].

One of the main causes of high mortality and morbidity rate is a lack of proper diagnostics and treatments, which are usually too expensive and time-consuming, providing results in up to 2 weeks.

Furthermore, the application of empiric antimicrobial therapy involves a misuse and overuse of antibiotics, resulting in a startling increase of antimicrobial resistance (AMR). Such process represents a global issue, and if action is not taken in time, it will surely worsen and claim millions of lives in the coming years. On this regards, O’Neill in his *"Review on antimicrobial resistance"* [15], stated that 700000 people die of resistant infections every year, and that this assessment will grow to 50 millions by 2050. Indeed, the possible consequences raising from the ineffectiveness of antibiotics are incredibly alarming, due to their wide use in most medical procedures. Moreover, a correlated issue is the increase of public health-care expenditures that every country is compelled to bear in the next future, hence 100 trillion USD a year should to be taken into account in 2050, according to O’Neil [].

Concerned by that, the governments of several countries have started to tackle emerging infectious diseases and AMR. However, such problem can only be solved with an international collaboration, because of the high risk of microbes to easily spread worldwide.

Accordingly, new technologies are sorely needed to promote rapid diagnostics, which not only would allow optimal treatment decisions in a short time, but also would reduce the unnecessary use of antimicrobials. A promising solution is represented by the Lab-On-Chip (LOC) Technology, which develops miniaturised devices that integrate and automate single or multiple lab processes on a single chip.

1.2 Background

The Lab-on-Chip (LoC) technology provides integrated devices able to perform biochemical analysis onto a single chip. Several applications are involved, including medical diagnostics. The LoC systems are based on the use of microfluidics, which allows the miniaturisation of the dimensions. There are many benefits arising from the use of this novel technology, firstly the decrease of the analysis time, the reduction of the reagent consumption, the ease of use, and also the high sensitivity and specificity. All of these seem very appealing for the realisation of point-of-care diagnostic systems, in particular in resource-limited settings. According to the WHO, the guideline to follow in order to have a successful POC device is the ASSURED criteria:

- Affordable.
- Sensitive.
- Specific.
- User-friendly.
- Rapid and robust.
- Equipment-free.
- Deliverable to end-users.

These devices and their implementation need to be cost-effective, especially in the underdeveloped areas of the world where there is no access to expensive laboratory facilities. Therefore, it is preferable to consider disposable and portable chip, that doesn't need a specific supporting equipment. It is also crucial that these devices can be used by non-professional operators so that only a minimal training is required. The time for the test should not exceed 30 minutes and the shelf life guaranteed should be at least of 24 months without the need of any refrigeration. Another requirement is the realisation of battery-powered systems independent from the electricity supply. Furthermore, in order to permit an early detection of infectious diseases the LoC diagnostic systems need to be characterised by a very high sensitivity and specificity.

The three current methods mostly implemented to detect infectious disease are:

1. Culture-based microscopy.
2. Molecular method.

3. Immunoassays.

The microscopy still remains the gold-standard in diagnostics pathology, but does have its limitations, for instance it provides results some weeks after the test and requires a specialised equipment and expert operators. With the employment of Molecular methods, also known as NAATs, the results are instead ready after a few hours and it is possible to obtain a very sensitive and specific quantitative detection. Although, in the same way as the previous one, high-cost lab facilities are necessary to read the results. Another drawback is the requirement of sample processing before starting the measurement. On the contrary, the immunoassays use raw sample for the detection, allowing a reduction of the entire cost of the test. Nowadays, these low-cost, rapid and easy to use assays represent the most common tests available on the market as kit formats. Acknowledged examples are the lateral flow tests, such as the home pregnancy test, which are paper-based devices using capillarity to transport fluid. Nevertheless, immunoassays produce qualitative diagnosis that are not sensitive enough. So, in order to grant an high specific, high sensitive, rapid, affordable, portable and quantitative detection it is necessary to develop a novel tool which brings together the benefits of the molecular method and the benefits of the immunoassays. All this is possible with the LoC technology.

Chapter 2

Overview of the LoC platform for POC infectious disease diagnostics

The diagnostic tool presented in this chapter was developed by the research group of Dr. Pantelis Georgiou in the Centre for Bio-Inspired Technology at the Imperial College of London. It consists in a CMOS-based Lab-on-Chip platform able to detect infectious disease at an early stage by monitoring on-chip DNA amplification of pathogens. The novelty of this platform is based on the simultaneously use of microfluidics, microelectronics and molecular methods. Such an approach can rapidly provide highly sensitive and specific diagnosis, so to enable a virus detection even before the onset of the disease. The application of early and specific treatments would thus be possible. Furthermore, this would avoid any increase in the antimicrobial resistance, by distinguishing among different infectious diseases with similar symptoms. Also, this automatic and fully integrated diagnostic tool is independent of the operator's skills, and highly improves efficiency and reliability of test results. Such characteristics can be quite important and useful to the application of these portable devices in the developing countries.

The employment of Molecular method, based on DNA amplification, within a LOC, allows a quantitative and high sensitive detection in an extremely fast format ($<$ 15 minutes from sample to results).

The possibility of handling a small amount of fluid not only would enable a better control of the molecular concentration and interaction, but it would also reduce the reagents' costs and the chemical waste, and save precious time needed for the analysis. One of the most challenging aspects in the realisation of a POCT is the integration of the sample preparation process. To this end, a Microfluidic System is decisive, enabling the DNA extraction from a body fluid and the optimisation of its interaction with sensors without the need for complex and expensive laboratory instruments.

There are also many benefits from the use of microelectronics. Semiconductor technology through integrated ISFET sensors in CMOS enables the creation of a label-free, non-optical and real-time detection platform. Additionally, this facilitates the realisation of low-costs, easy to read, portable and scalable devices.

To sum up, the three novel approaches considered are:

- Nucleic acid amplification chemistries (LAMP).
- Microfluidic technologies.
- Biosensing technologies (CMOS-based arrays).

2.1 Nucleic acid amplification chemistries

2.1.1 PCR

The PCR is a well-known molecular method which enables the amplification of a specific DNA sequence. It represents an essential step to detect the pathogens potentially present in a sample because their DNA amount is very low. The PCR provides indeed millions of identical copies of DNA starting from just a few ones in a very short time. DNA is a nucleic acid composed by single monomers called nucleotides, which are made of a sugar (desoxyribose), a phosphate group and a nitrogenous base (adenine (A), uracil (U), guanine (G), thymine (T), and cytosine (C)). In biology, the DNA is in form of a double helix in which two chains are solidly entwined. The backbone is made of an alternation of sugars and phosphates, while the nitrogenous bases are turned inward and match together through hydrogen bondings according to the base paring rule (see Figure 2.1).

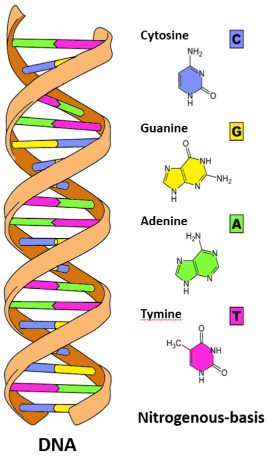

Figure 2.1: Double helix DNA.

The PCR works thanks to a DNA polymerase, which is an enzyme able to synthesise a DNA strand adding nucleotide by nucleotide. Before the replication can take place, it is necessary to separate the two strands, or in other words denaturate the DNA, using them as templates. The polymerase is not able to initiate the syntehisis of a DNA strand but can only extent a pre-existing strand. In order to do that, it is essential that a *primer*, which is a short RNA fragment, is already paired to the template. The primers are specific for the target DNA sequence and are usually chemical synthesized and made of 15-20 nucleotides.

Consequently, the enzyme first links to the single strand DNA, then starts to add free nucleotides to the 3' end of the primer. The PCR consists so in three phases, the *denaturation*, the *annealing* and the *extension* (see Figure 2.2). To switch from one to another a temperature change is required.

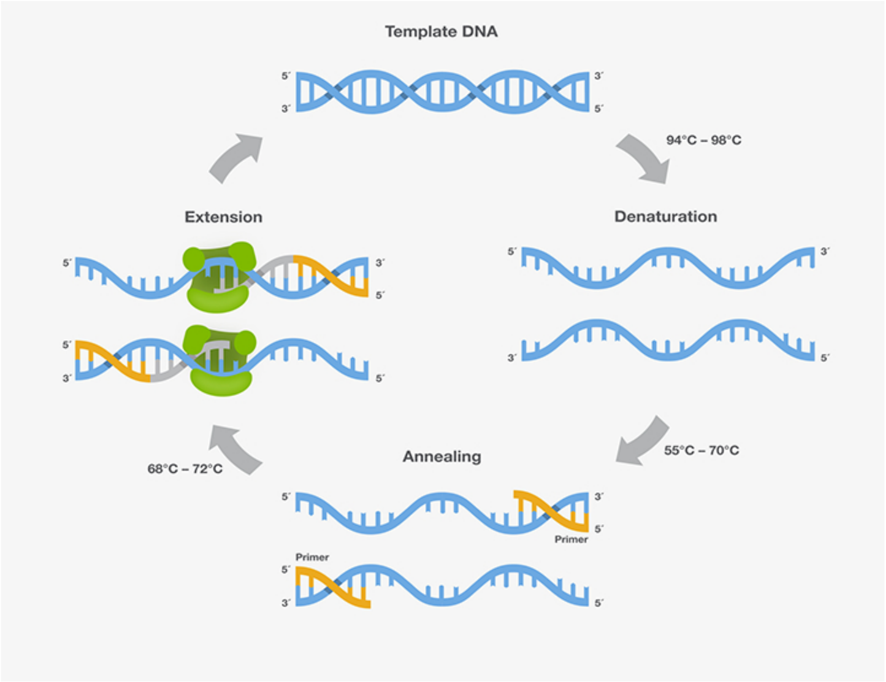

Figure 2.2: PCR cycling steps [6].

Denaturation : the separation of the two DNA strands is achieved by heating; in fact the increase of temperature causes the disruption of the hydrogen bonds between the nitrogenous bases. In this phase, the DNA solution is heated to over the melting temperature (T_m) of the DNA. The T_m is defined as the temperature at which the 50% of a DNA sequence is hybridised from its complementary strand (see Figure 2.3). This process, also known as "DNA melting", is associated

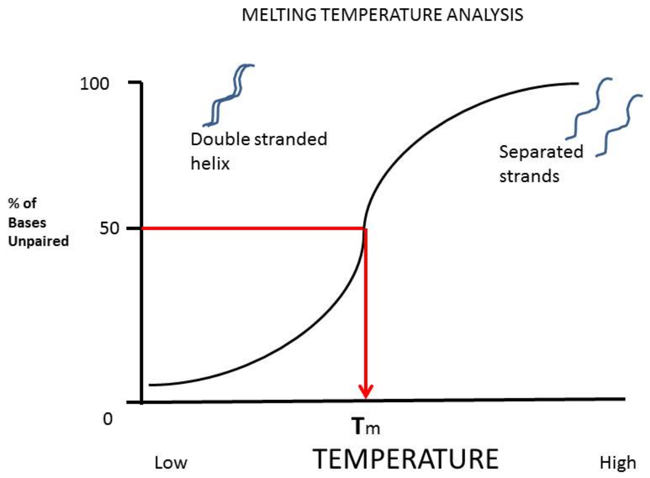

Figure 2.3: DNA melting curve.

with a reduction of the viscosity and an increase of the 40% absorbancy at 260nm (see Figure 2.4). Usually the temperature considered in this phase ranges from 94°C and 98°C.

Annealing : The primers link to the 3' ends of the target DNA sequence, hybridising the two single stranded templates. The annealing temperature T_a is lower than T_m and needs to be optimised according to the length and nature of the primers. It has to be low enough to allow the bond primers-template and high enough to grant a specific hybridisation at the same time . Commonly, the T_a is around 50-60°C. The annealing time t_a is another important parameter, that needs to be set carefully in order to avoid unspecific pairings, and is usually of 20-30 seconds.

Extension : The polymerase starts the polymerisation in direction 5'→ 3' recruiting dNTPs. The temperature between 68-72°C promotes the polymerisation process. The DNA-polymerase considered is the *Taq* polymerase, which is a termostable enzyme isolated from a thermophilic bacterium and able to withstand high temperature.

At the end of each cycle two copies of the target DNA are generated. It is possible to obtain thousands to millions copies starting from only few copies by repeating the cycle several times. Thus, the amplification follows an exponential trend:

$$N = (1 + e)^n \tag{2.1}$$

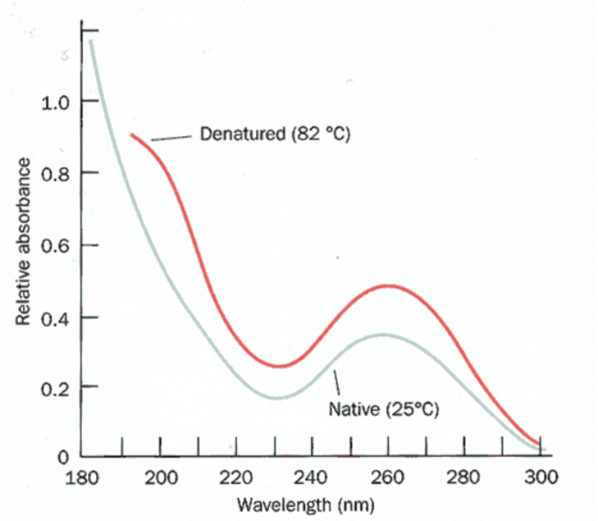

Figure 2.4: DNA Absorbance Spectrum.

where N is the number of the duplicated copies at the end of the reaction, e represents the efficiency and n is the number of repeated cycles. The PCR has three different stages (see Figure 2.5) depending on the reaction rate, which is influenced by a number of factors, such as the reagents availability and the enzyme stability. At the beginning of the reaction, in the *exponential* phase of the amplification curve, e is assumed to be almost equal to 1 and so the number of copies is doubled at each cycle. After that, the *linear* phase begins and, considering that the supply of reaction components starts to decrease, the amplification slows and becomes less specific and precise. Finally, there is the *plateau* phase at which the reaction stops [16] [7].

The traditional PCR employs the agarose gel electrophoresis to evaluate the PCR products at the end of the reaction. In the real-time polymerase chain reaction (Real-Time PCR) it is instead possible to monitor the DNA amplification while the reaction is in progress. In this case the detection method is based on fluorescence and can be specific or not for the DNA target sequence. In general, the *exponential* phase provides the best conditions to take measurements, since it represents the more specific stage of PCR.

To implement a PCR is then necessary to have a sophisticated equipment, such as a thermal cycler, that is able to carry out consecutive thermal cycles and to detect the fluorescence emitted during the reaction. Indeed, it is required a sensitive control (±0.5°C) and a rapid change (10°C/s) of temperature and also a good sealing to avoid the evaporation of the sample when high temperature is reached (100°C) [8].

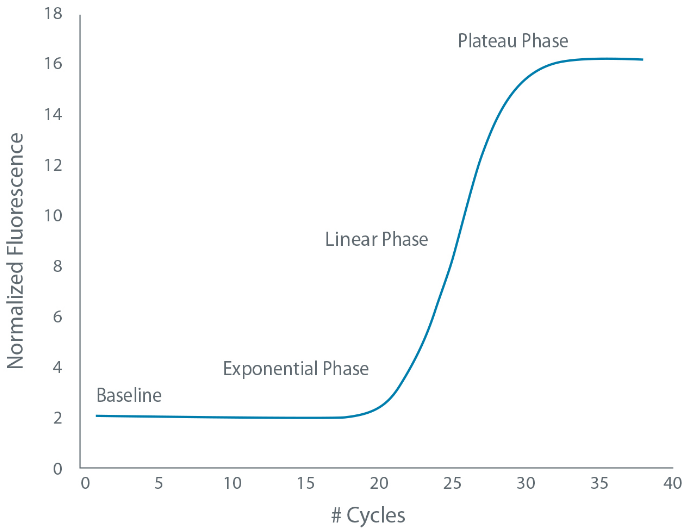

Figure 2.5: PCR amplification stages [7].

2.1.2 LAMP [1]

The needs for simplicity led to the development of *isothermal* methods, i.e., methods that are able to amplify the DNA at a constant temperature avoiding the such a complex thermal cycling. The LAMP is the most common isothermal PCR, and is already widely used in many POC-tests. It was developed by Notomi *et al.* [1] in 2000, and not only has proven to be of much simpler implementation than a traditional PCR, and to not require expensive instrumentation, but also to be characterised by high selectivity, rapidity and efficiency. The LAMP offers many advantages:

- High sensitivity, with a detection limit of few copies (similar to PCR).
- The presence of cauliflower-like structures as reaction products makes the detection simple, easy and selective.
- High specifity, thanks to the employment of a set of four primers recognising six indipendent sequences on the target DNA.
- Extreme rapidity, enabling an amplification from few copies to 10^9 in less than an hour.
- No need of expensive instruments for the thermal cycling.
- The low temperature involved (around 37-65°C) reduces evaporation and air-bubbles formation, and so prevents sealing problems and minimizes the energy consumption in heating [8].
- Possibility to amplify RNA sequences with high efficiency.

The LAMP requires a DNA polymerase and four primers, that are specially designed in order to recognise the target DNA by six distinct sequences. They are divided in two groups, the *inner* primers, further divided into forward inner primer (FIP) and backward inner primer (BIP), and the *outer* primers, further divided into forward outer primer (F3) and backward outer primer (B3). The reaction is described in three steps, the *starting material producing step*, the *cycling amplification step* and the *elongation and recycling step*. The *outer* primers participate only in the first step, while the *inner* are employed for the entire time of reaction. The mechanism of reaction is illustrated in Figure 2.6:

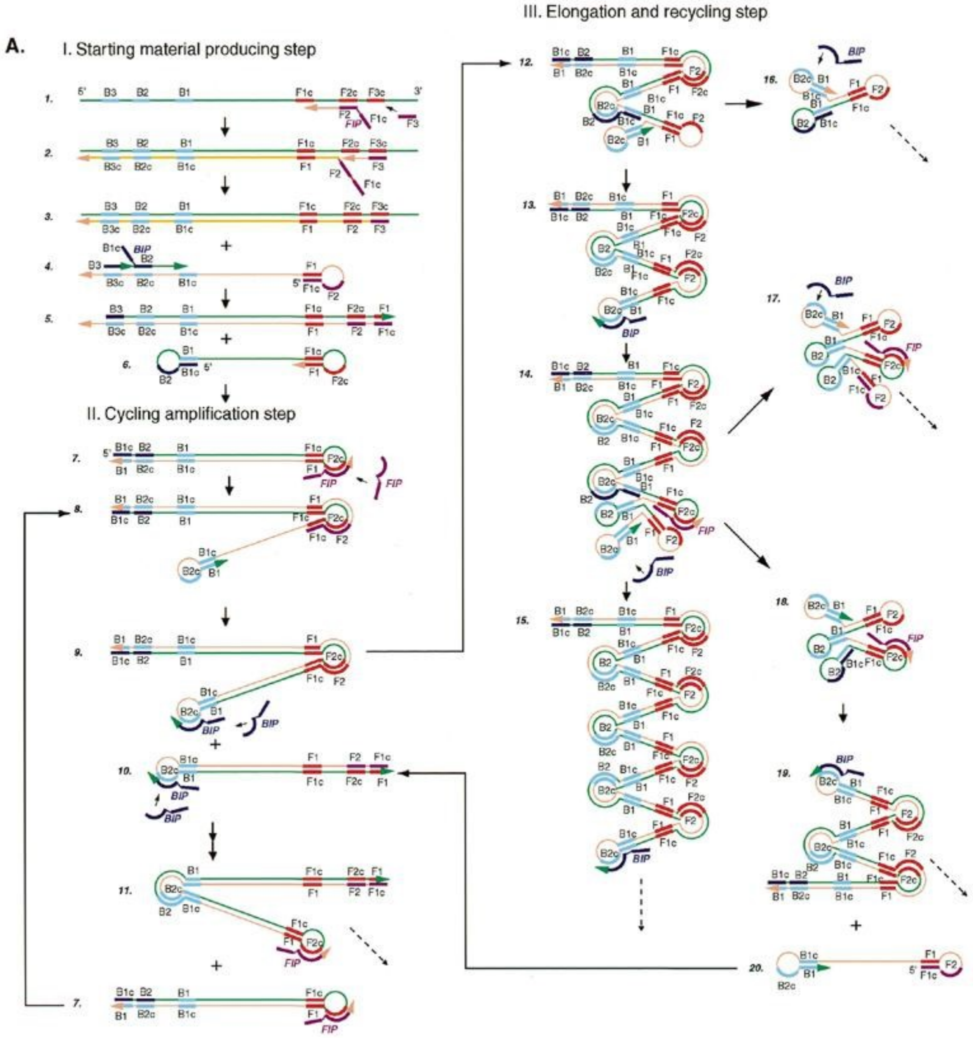

Figure 2.6: Schematic representation of the mechanism of the LAMP [1].

During the LAMP, the continuous strand displacement and the self-annealing produces single stranded looped structures. Each inner primer is made of two sequences of sense and antisense strands of the target DNA, linked by a TTTT spacer. To start the reaction, the temperature is increased around 65°C to heat denaturate the DNA sample. The *Bst* DNA polymerase used in the LAMP is characterised by a major tolerance than the *Taq* polymerase, making the LAMP less sensitive to inhibitors than the PCR [8]. The duration of the entire reaction is usually of 1 h.

The amplification is initiated by one of the inner primers that hybridizes the target DNA and gives the start for the DNA synthesis, while the following displacement is caused by an outer primer. Once the new single-stranded DNA is primed by the second inner primer on the opposite end, it is used as template for the next amplification. As a result a stem-loop structure is formed. In the following steps the inner primer hybridizes again the single-stranded DNA and the subsequent displacement by the second outer primer leads to the formation of a double-looped structure, termed *lamp dumb-bell structure*, which represents the start structure for the second stage of the LAMP. In the cycling stage the DNA synthesis starts not only from the annealing of the two inner primers but also from the self-annealing, which consists in using the self-structure of DNA as a template. This stage finishes with the generation of structures of different length made of alternately inverted repeats of the target sequence on the same strand [17]. In the last step, the cycling step is repeated several times, doubling the stem length of the stem-loop at the end of each cycle.

Lastly, all the benefits introduced by the LAMP make this method an extremely interesting diagnostic tool for POC application, especially with regard to minimal instrumentation [8].

2.2 Microfluidic technologies

"Microfluidics can be defined as the study of flows that are simple or complex, mono- or multiphasic, which are circulating in artificial microsystems, i.e. systems that are fabricated using new technologies" [18]. Microfluidics developed in the 1900s as a consequence of the progress made in the field of miniaturisation. Today microfluidic systems are widely used in different fields and are being used for the realisation of novel medical devices. Indeed, microfluidic technology has paved the way for scalable and fully integrated POC testing.

In traditional genomyc analysis, before starting the DNA amplification, three steps are required: (i) cell lysis (breaking down of the cell membrane), (ii) cleaning and purification (from lipids, proteins and RNA), and (iii) elution (extraction and purification of the DNA from the lysate). For a bloody test, there is also an additional step that separates the plasma from the whole blood. The Figure 2.7 depicts a common work flow for a NAATs molecular diagnostics, where the sample processing is followed by the DNA amplification, and finally by the detection. The entire sample preparation process, usually performed in a lab that requires a complex labor, can be directly implemented within a POC device thanks to a microfluidic cartridge. This is the ultimate goal of the design of a Lab-on-Chip (LoC), a device able to detect biological target directly in a raw sample. The progress in the miniaturisation field was also driven by the possibility to obtain a low-cost diagnostic tool. In fact, microfluidics employs a low reaction volume, and enables the development of inexpensive POC devices, since the reagents's cost represents almost the 50% of the total cost of the device. However, another important issue needs to be addressed, considering that large volumes allow the detection of analytes at low concentration (few copies/ml) [8]. The reaction volume (V) is indeed a critical parameter, and its relationship with the concentration of the analyte is described by the following equation:

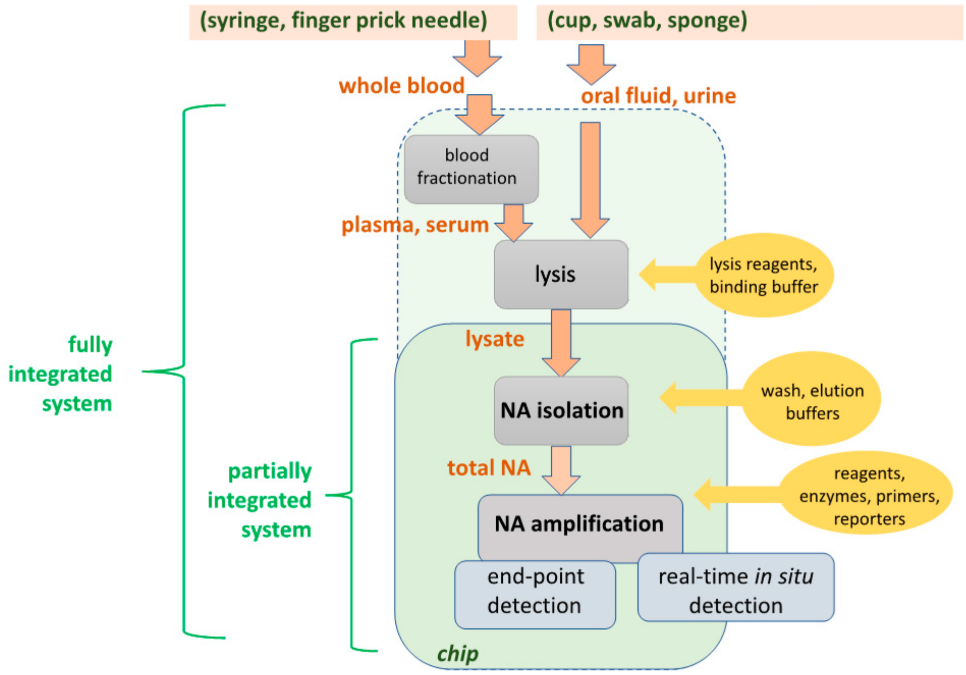

Figure 2.7: Processing steps for a a NAATs molecular diagnostics [8].

$$V = \frac{1}{\eta_{\mathrm{s}} N_{\mathrm{A}} A_{\mathrm{i}}} \tag{2.2}$$

where η_s is the efficiency of detection ($0 < \eta_s < 1$), N_A is the Avogadro's number (6.02×10^{23}) and A_i is the concentration of the analyte i in the sample [19]. So, a lower volume is necessary with the increasing of the analyte concentration and considering better sensors. A good compromise considers a reaction volume of about ten μl.

Moreover, the automation of the entire process reduces the risk of contamination and enhances the reliability and the high-throughput of the test. Microfluidics offers also the chance to overcome the limits of the current standard diagnostic methods, making possible the performing of multiplex analysis [20]. The detection of multiple targets is essential to provide healthcare of real-time information that are crucial to determinate the appropriate treatment strategy. Infectious diseases present sometimes similar symptoms and in order to have an accurate diagnosis it is imperative to know which pathogen is causing the infection in a host. In such a way, it is possible to evaluate the state of the disease, the efficiency of a treatment and the drug resistance as well [20]. In order to perform multiplex detections, it is fundamental to perform concurrently amplification reactions in parallel. To address this need, a microfluidic chip represents a promising solution, since it allows the compartmentalisation of the sample fluid in multiple chambers within a diagnostic device. All those advantages made the microfluidic research grow impressively, and will lead to a further progress in the next future. According to the Lux Research [21], the health care microfluidic market will grow at 13% annually, reaching nearly 4 billion in 2020.

2.2.1 A State-of-the-Art review of compartmentalisation approaches in Microfluidics

In order to design a simply and cheap device, the microfluidics tents to avoids the employment of "moving parts", that are technically challenging. There are several approaches which allow the fluid compartmentalisation without the use of valves and pumps. *Water in oil microdroplet* approach (see Figure 2.8) is one of these and it has been chosen by many research groups. It considers an immiscible fluid, an oil phase, to break the continuous flow of the sample solution in a discrete one. Most of these microfluidic devices were made in polydimethylsiloxane (PDMS) and fabricated by standard soft-lithography and adopted different loading methods. Yayun Fu *et al.* [22] proposed a “glass-PDMS-glass” sandwich system containing 10000 reaction compartments of $0.785nl$ each (see Figure (a)). This strategy uses the difference of air pressure inside and outside the chip. Thanks to the high permeability of PDMS, the device is degassed and a negative pressure is generated within the device, that sucks the solution from the inlet port inside the channel. To emphasise the process a PDMS pump on the outlet port is also considered. Thompson *et al.* [23] developed instead the Self-Digitization (SD) Chip (see Figure (b)), that presents a serpentine design containing 1020 chambers. In this case, the differential pressure along the channels that drives flow was created through a pipette and a vacuum pump. Lastly, Yamada *et al.* [24] presented the ‘oil microsealing’ concept (see Figure (c)), that consists in sealing and isolating the sample solution inside the microchambers by filling the microchannels with oil. The permeability of the PDMS to the gas was used to push out the gas out during the loading of the solution. To achieve that it was necessary to consider a plug to close the outlet port and the application of 300 mbar gauge pressure on the inlet.

The *SlipChip* (see Figure 2.9) is a microfluidic device in glass designed by Ismagilov group [9]. It is made of two layers in close contact, each of which has various wells. The wells of the bottom plate were preloaded with different reagents. The SlipChip has two configurations:

- In the first one, the wells of the top plate connect the ducts of the bottom plate into a continuous fluidic path, enabling the loading of the sample (by a pipettor).
- In the latter, the top plate is slipped relative to the bottom plate to align the sample-containing wells of the top plate with the reagents-containing wells of the bottom plates. Diffusion between reagents and DNA sample is then possible and the reaction occurs.

A silanisation with fluorocarbon was used to make the surface of the glass hydrophobic and fluorophilic and to facilitate the relative motion between the two plates. This device is realised by standard photolithography and wet chemical etching. The Ismagilov group developed also a 3D-printed pumping lid [25] to create positive and negative pressures inside the microfluidic device *via* controlled compression or expansion of gases, with the purpose to achieve an equipment-free pumping operation.

The *EWOD phenomenon* is one of the most common actuation mechanisms used in digital microfluidics (DMF). It refers to the ability of an applied voltage to modulate the “wettability” of a surface, and to cause so the spreading of aqueous droplets [26] (see Figure 2.10 (a)). In the EWOD devices the droplet pathways consist of contiguous electrodes, which connect different areas of the chip. These electrodes can be used either simply for transport or for other more complex operations such as mixing and splitting. According to the model proposed by Gong *et al.* [27], the droplets are formed from an on-chip reservoir in three steps (see Figure 2.10 (b)):

1. A liquid column is extruded from the reservoir by activating a series of electrodes adjacent to it.
2. Once the column overlaps the electrode on which the droplet is to be formed, all the remaining electrodes are deactivated to form a neck in the column.
3. The electrode in the reservoir is then activated to pull the liquid back and break the neck completely to form a droplet.

Since the liquid droplet is sandwiched between two hydrophobic (Teflon AF-coated) plates (see Figure 2.10 (c)), an oil film is used for the isolation,

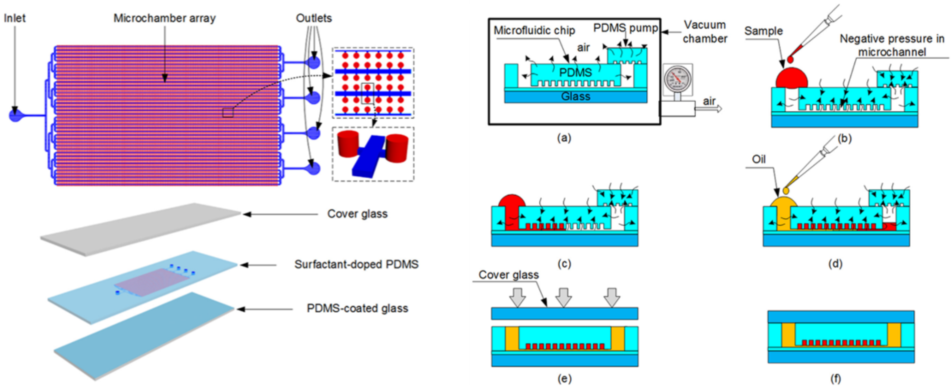

(a) *Microfluidic device proposed by Yayun Fu et al. [22].*

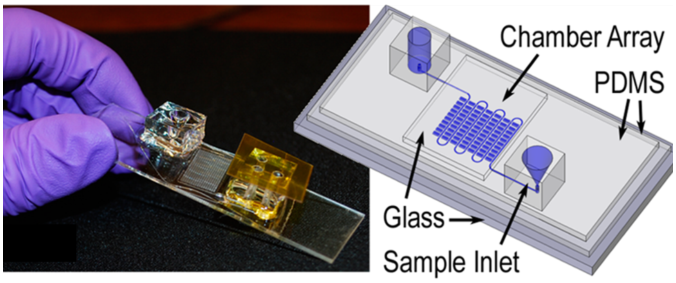

(b) *Self-Digitization (SD) Chip [23].*

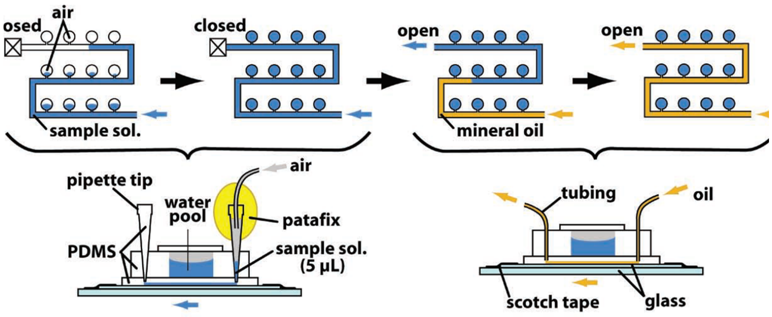

(c) *Microfluidic device proposed by Yamada et al. [24].*

Figure 2.8: Water in oil microdroplet approach.

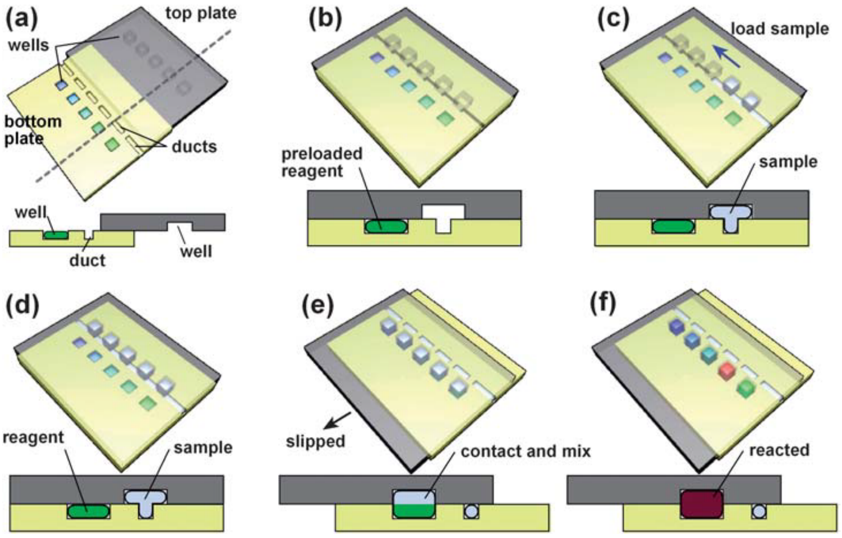

Figure 2.9: Slipchip device [9].

minimising protein adsorption and facilitating transport. Nevertheless, traditional EWOD devices require an external high-voltage supply (of 40-80 V) and a switching circuitry. It is also important to control the volume of the droplet. To accomplish that goal, the measurement of the droplet footprint area is performed in the evaluation of the capacitance between the electrodes on the top and bottom plates, and by multiplying the value obtained with the height of the gap between the two plates.

The *DEP*-based systems use electric field for the fluid transport (see Figure 2.11). Indeed, given a polarisable particle, the induced electric dipoles align themselves parallel to the applied electric field. If the electric field is not uniform, each half of the dipole experiences unequal Coulombic forces, resulting in a net force imposed on the particle. The particle can be then pushed towards/off the regions of strong electric field depending on whether the particle is more/less polarisable than the suspending medium. The electric field gradients, which are essential to induce DEP forces, are generated by 2D or 3D microelectrodes. The 2D microelectrodes are normally patterned within the bottom of the microchannel using conventional lithography techniques [28]. Since DNA exhibits a negative charge, DEP can be used for its capturing and characterisation. Morales *et al.* [29] proposed a continuous microfluidic device for DNA-trapping which involves the DEP motion. Integrated coplanar electrodes running axially are used along the length of the channel to apply a transverse uniform DC electric field. Depending on the ionic strength of the selected buffer, the DNA sample could be concentrated by electrophoretic forces at the positive bias electrode or trapped at an equilibrium position within the channel, in which the electrophoretic (EP) force and the drag force generated by an induced electroosmotic (EO) flow are

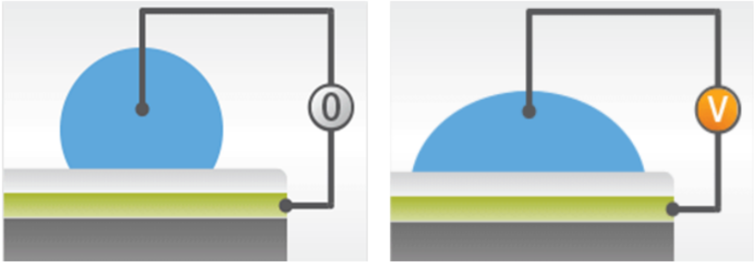

(a) *EWOD phenomenon [26].*

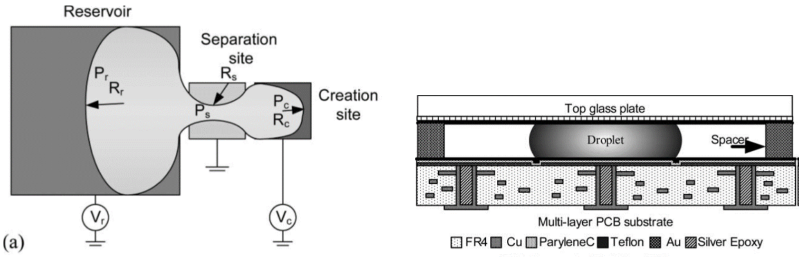

(b) *Voltage control of droplet creation process on EWOD device [27].*

(c) *Cross-sectional view of the EWOD chip [27].*

Figure 2.10: EWOD approach.

balanced.

Microfluidic large scale integration (LSI) platform is an approach based on microfluidic valves. The most important example is the $NanoFlex^{TM}$ valve (see Figure 2.12), which is made of a planar glass substrate and two layers of PDMS on top of it. The lower elastomer layer contains the fluidic ducts and the upper elastomer layer features pneumatic control channels. Due to the high elasticity of PDMS, the control channel squeezes the lower elastomeric layer, and blocking the liquid flow, when a pressure p is applied to it. The size of these valves is of the order of 100 x 100 μm. So, a simple

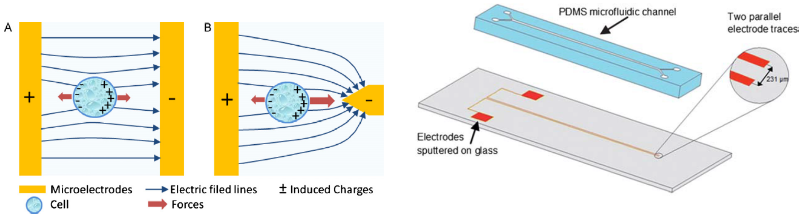

(a) *Response of a polarisable particle to (A) uniform and (B) non-uniform electric fields [28].*

(b) *Microfluidic chip proposed by Morales [29].*

Figure 2.11: DEP approach.

microfluidic array can be designed, in which each fluid channel is controlled by its own individual valve control channel. This microfluidic multiplexer allows control of n fluid channels with only $2\log_2 n$ control channels. However, this approach requires the actuation by external pneumatic controllers [10].

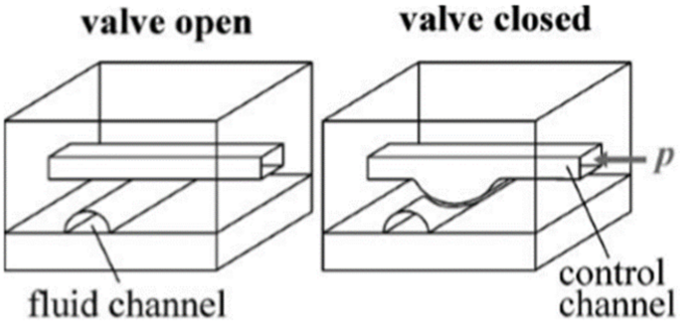

Figure 2.12: $NanoFlex^{TM}$ valve [10].

2.3 Biosensing technologies

Most of current POC molecular diagnostics systems use optical-based methods for the detection of the amplification products. These methods usually employ intercalting dyes, such as $SybtoGreen^{TM}$, able to insert themselves inside the double helix during the amplification reaction. In this way, once the sample solution is illuminated with a LED at a certain wavelength, in the ultraviolet or blue range, the dyes emit light at a longer wavelength in the visible region. The fluorescence intensity is then related with the amount of the DNA copies and so it is possible to monitor the progression of the reaction. Another approach performs absorption measurements after the precipitation of product causes turbidity. An alternative is represented by the lateral flow strips which use immobilised antibodies to capture specific labeled amplicons [8]. All these methods require then complex sample processing steps before the isolation and the detection. Also, since these tests are performed by a skilled personnel in laboratory facilities, they are quite expensive and difficult to scale. With the aim of realising a single fully integrated scalable platform, it is vital to simplify the genetic tests, to make them low-cost, fast and scalable. In this prospect, semiconductor technology provides label-free, non-optical, real-time simultaneous amplification and detection of genetic targets. This is based on the use of ISFET, chemically sensitive sensors enabling the measurement of the variation of ion concentrations in solutions. Such an innovative detection approach can be used to design a pH-sensing device able to quantify the DNA amplification.

In fact, during the polymerisation of a new DNA strand, the polymerase releases protons (H^+) in solution causing a decrease of the pH:

$$DNA_{\mathrm{n}} + dNTP = DNA_{\mathrm{n+1}} + PP_{\mathrm{i}} + H^+ \tag{2.3}$$

where dNTP is a nucleoside triphosphate and PP_{i} is the pyrophosphate. More specifically, the change in ion concentration causes a variation of the floating gate voltage V_{gs} of the device by a an additional potential called V_{chem}:

$$V_{\mathrm{chem}} = \gamma - \alpha S_{\mathrm{N}} log([H^+]) \tag{2.4}$$

where γ gathers constant parameters which are independent on the ion concentration, and α represents the deviation from the Nernstian sensitivity (S_{N}= 59 mV) [30] [2]. There are numerous benefits resulting from the employment of this detection method:

- Scalability.
- Repeatability.
- Low cost.
- No labeling.
- No optics.
- System Integration.

A commercialised example which uses the semiconductor technology is *LiDia*^{TM} Bloodstream Infection Test (*LiDia*^{TM} *BSI*) by DNA Electronics, able to identify pathogens and key resistance markers directly from whole blood [31]. All the capability of such intelligent sensing listed above has driven Dr. Georgiou's research group to develop a novel integrated ISFET analogue sensing and digital memory array designed as a full SoC and embedded in a Lab-on-Chip platform (Figure 2.13) [2]. This integrated platform can significantly speed the decision making at the point of need and so tackle the outbreaks of a disease in time.

2.3.1 CMOS-based pH sensing platform [2]

The LoC presented in this work considers a 0.35 μm CMOS technology that integrates an analogue sensing and a digital memory array. The array of 78×56 pixels capable of ion imaging is used for pH sensing to measure the amount of DNA copies while a LAMP reaction is running. The in-pixel memory cells are used to encode the ion concentration in time and to store a calibration value for the biasing of each pixel. This digital approach not only offers the possibility to scale the system, which represents a key aspect with the prospect of fabricating these systems on large-scale, but also improves

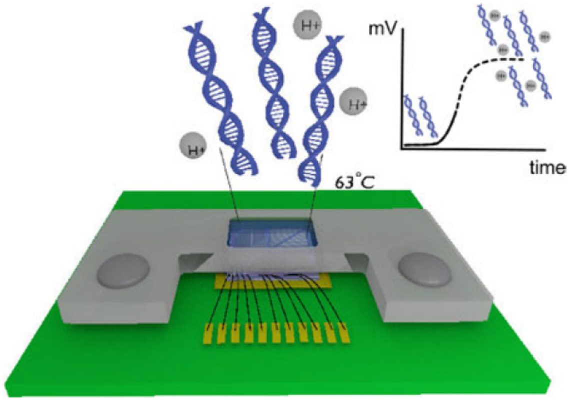

Figure 2.13: The CMOS platform is used for on-chip real-time amplification and detection of DNA. [2]

the chemical coupling and achieves an unprecedented outstanding Signal-to-noise ratio (SNR) (34.16 dB).

The Figure 2.14 shows a microphotograph of the array that occupies the left side of the chip. This consists of 3874 chemical pixels and 494 temperature pixels. Each temperature sensor is placed at the center of 9 chemical pixel clusters and allows the monitoring of the temperature. The regulation of the temperature is indeed a very critical aspect for a successful LAMP reaction.

The Figure 2.15 shows instead the full Lab-on-Chip platform. The assembly of the chip is described by the following steps: (i) the 4x4 mm die is glued on the ground plane of a 65×50 cm PCB cartridge, (ii) the wire bondings for the analogue and digital connection are covered by a bio-compatible epoxy, (iii) a Peltier device is placed on the bottom of the cartridge as a heater, (iv) the cartridge is plugged in a motherboard. The motherboard provides the power supply and is responsible for the data aquisition and biasing. Furthermore, in order to grant a constant temperature during the reaction, the on-board microcontroller (MCU) allows a temperature regulation, adjusting the value of the voltage applied to the Peltier according to the readouts from the temperature pixels. The platform is able to perform an automatic calibration of trapped charge, achieving 95% pixel efficiency with 4% standard deviation. The pH sensitivity is of 3.31 μs/pH at the calibrated value of 10 μs. The Table 2.1 shows the main features of the system.

The platform was demonstrated as a POC device for infectious disease diagnostic, performing on-chip realtime DNA amplification and detection. In particular, a LAMP reaction for a lambda phage DNA was run. A 12μl of sample solution was loaded inside a reaction chamber within an acrylic manifold screwed on the top of the chip. This manifold was obtained from an

Figure 2.14: Microphotograph of the ISFET array [2].

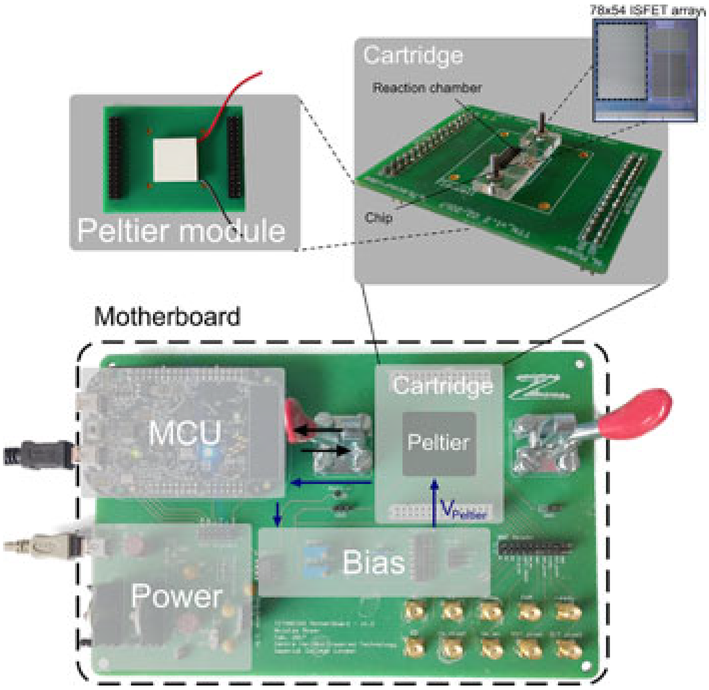

Figure 2.15: Description of the block-level implementation of the full Lab-on-Chip platform [2].

Technology	AMS 0.35 μm
Pixel size	37μm $\times$ 31μm
Chip size	4mm $\times$ 2mm
Number of chemical pixels	3874
Number of temperature pixels	494
Maximum drift rate	6.5 mV/min
Offset compensation range	1 V
Pixels in range	95 %
Calibration	$\mu = 9$ μs, $\sigma = 370$ ns
pH sensitivity	11.91 mV/3.31μs for 1 pH @ 10 μs
Measured input referred noise	0.23 mV
Resolution of ADC	12.8 ns
pH resolution	0.019 pH
Power consumption	7.5 mW @ 3.3 V

Table 2.1: Performance of the system (adapted from [2]).

acrylic sheet thick 3 mm by laser cutting. The chamber was designed with the purpose of exposing the maximum possible surface area of the pixels.

Later, it was performed a calibration and the reaction started once the temperature raised 63°C. The pixel outputs were sampled continuously. To determine the reliability of the results, it was considered a triplicate of the experiment. Moreover, the results obtained on-chip were compared and validated with the results obtained after the performance of a pH-LAMP in a conventional real-time PCR instrument (Light-Cycler 96 System, Roche Diagnostics).

	Yield		pH	
	Pre	Post	Pre	Post
Neg	13.7	12.83	8.4	8.62
Pos	14.87	874	8.74	7.84

Table 2.2: DNA yield and pH variation [2].

The Figure 2.16 compares the obtained results. The two graphs show a very similar trend and are characterised by the same time-to-positive of 400 seconds, equivalent to less than 7 minutes. Instead, the table 2.2 shows the change in the averaged values of DNA-yield an the pH before and after the reaction in the PCR instrument, for both the positive and negative samples. The difference reported in pH was of 0.9. The platform's readout changes of 30 mV during the amplification, and this corresponds to a pH change of 2.22,

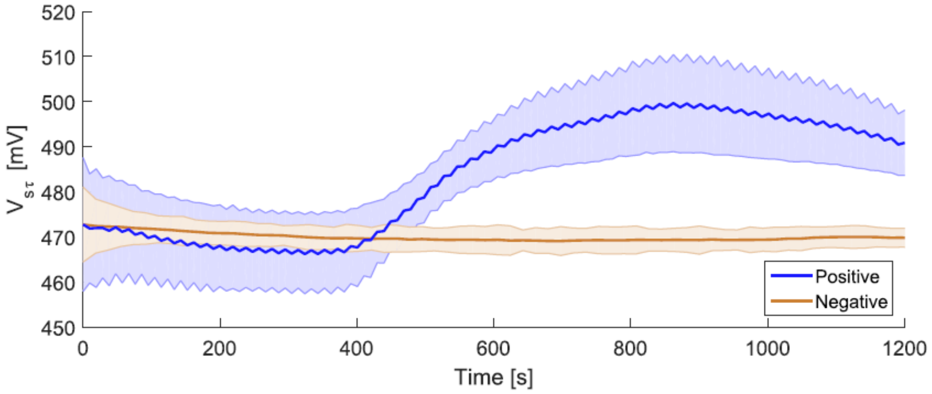

(a) *on-chip amplification*

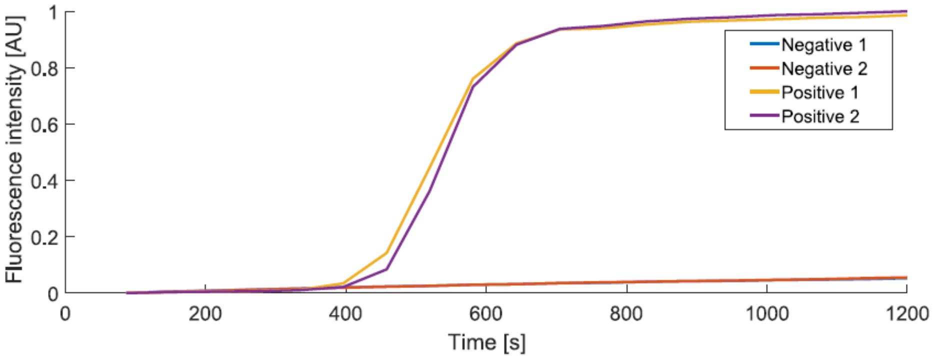

(b) *on-tube amplification*

Figure 2.16: Results for the DNA amplification in the benchmark instrument and on-chip [2].

confirming a high exponential sensitivity. This results demonstrate that the presented LoC is able to perform an high sensitive, specific and robust DNA detection through pH LAMP.

The performance of this device was further boosted thanks to the integration with a cloud network. The MCU transfers the data via Bluetooth to an AndroidOS application running on a smartphone, which is able to process them through appropriate algorithms (see Figure 2.17). The real-time remote monitoring makes the detection of outbreaks much more accessible in developing countries. One of the most critical consequences of a lack of a rapid detection method is the delay in the response by health authorities, causing the spread of the disease. A mobile diagnostic system is hence a promising solution to allow an early detection especially in remote areas, where the emergence of smart sensory systems is evident. The test results report is essential for the epidemiological mapping and infection management and control. Cause-of-death statistics help to determine where public health actions need to be addressed, reducing preventable deaths [32].

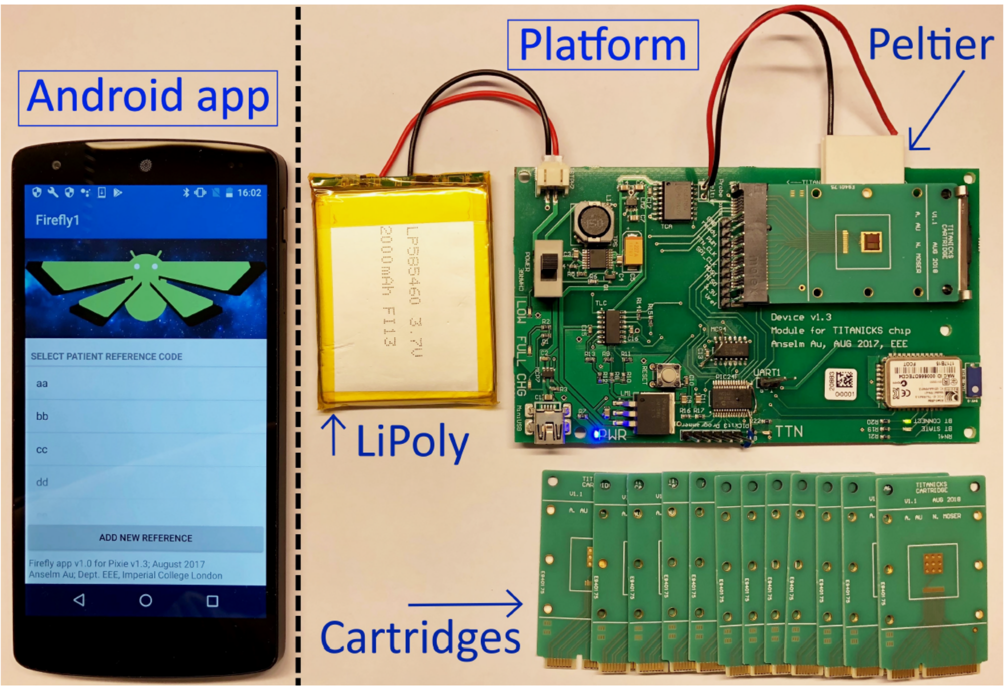

Figure 2.17: Android app (left); Platform (top right); Cartridges (bottom right) [2].

Chapter 3

Microfluidic Chip design and fabrication

The project presented in this report aims to the design of a microfluidic chip to be incorporated in the LoC platform described in the previous chapter. Thus, it is possible to propose a completely integrated device which enables the early detection of infectious diseases trough the DNA amplification of pathogens, using the pH LAMP reaction. In particular, the microfluidic cartridge strives to compartmentalise the DNA solution in four reaction chambers on the top of the chip, in order to conduct multiple analysis simultaneously. To satisfy the necessary requirements there are several challenges to overcome. The major difficulty was the realisation of a biocompatible device with micro-dimensions able to guarantee stability and repeatability in the measurements, avoiding any possible contamination.

3.1 Design

The SlipChip [9] was considered as a model for the operation method. The manifold was designed in SolidWorks, a 3D CAD design software. The Figure 3.1 shows the proposed model, which is made of two separated plates that need to sleep one on the top of the other.

The bottom layer (see Figure 3.2) has four reaction chambers where the LAMP occurs. The size of these chambers was optimised with the intention of exposing as many pixels of the array as possible. The chambers present an ellipse shape with a minor axis of $0.3mm$ and a major axis of $0.8mm$. Considering a thickness of $1.25mm$, the volume of each well is around $3\mu l$. This layer has also a channel and two wells, necessary for the loading of the solution. There are two through holes on the two sides to screw the manifold on the top of the microchip sensor. Moreover, in order to have a proper assembly with that chip, a squared recess was realised on the bottom side of the manifold to allow the housing of the die.

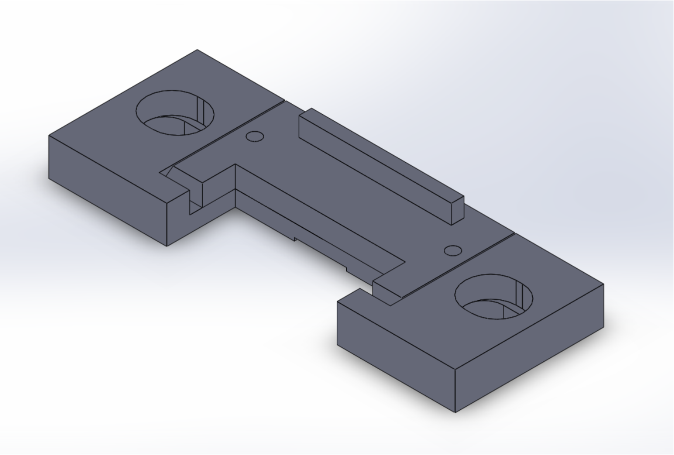

Figure 3.1: 3D model of the microfluidic chip.

The top layer (see Figure 3.3) presents an inlet and an outlet port of $1mm$ diameter, that have a conical shape to grant the insertion of the pipette used for the loading. Four wells with the same shape of the chambers in the bottom layer, enable the loading and represent the chamber in which the solution will be isolated. A little handle was also considered on the top to facilitate the motion between the two layers.

When the top and the bottom layers are aligned, the wells and ducts create a continuous fluidic path, that allows the loading of the solution. The serpentine design of the channel thus formed guarantees the complete filling of the reaction chambers before that the solution goes out through the outlet port. Instead, when the the top plate is moved down relative to the bottom plate, the fluidic path is disrupted and the wells on the top overlap the four chambers on the bottom. The solution is then isolated, and a sealed compartmentalisation is achieved (see Figure 3.4).

3.2 Fabrication

The fabrication technology adopted for the manufacturing is stereolithography (SLA) 3D Printing. This technique represents an good compromise between resolution and cost-saving, hence it is a good approach especially for the production in the prototyping stage. The SLA (see Figure 3.5) is an additive manufacturing process, that produces a 3D object building up material, layer by layer. The material is called photopolymer, since it is a liquid resin subjected to a photopolymerisation . In particular, the exposure to the light activates the photoinitiators, which are photosensitive molecules that upon radiation of light decompose into reactive species able to initiate the cross-linking of the monomers. As a result, the liquid resin becomes solid

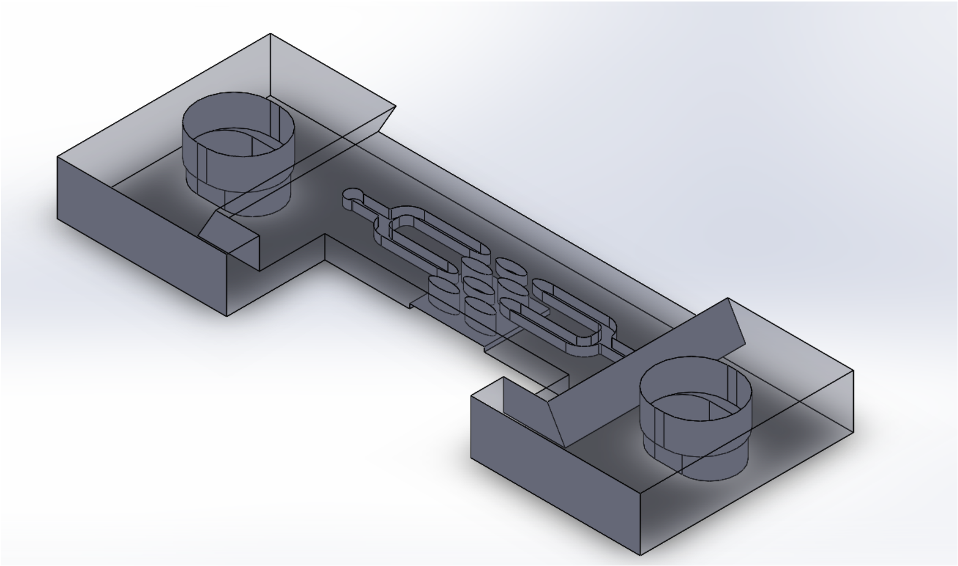

(a) *Isometric view.*

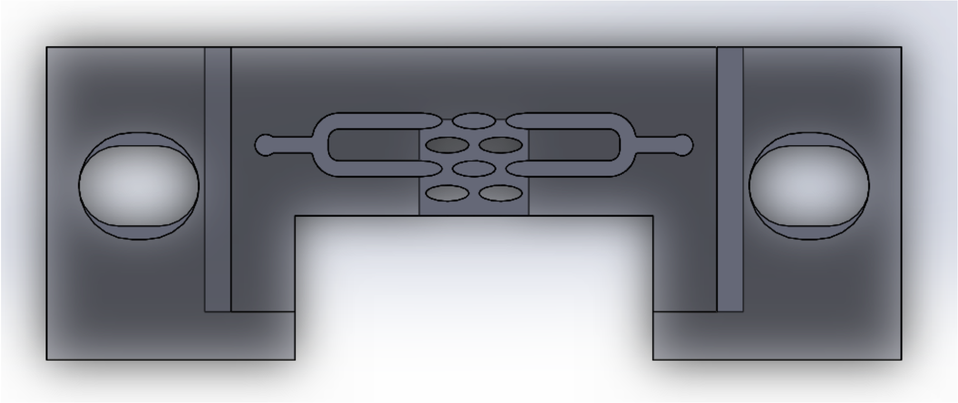

(b) *Top view.*

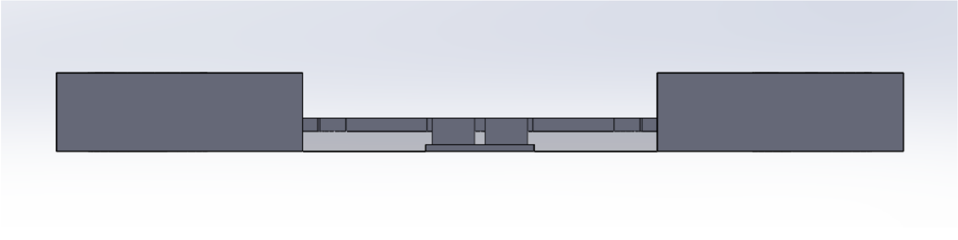

(c) *Front view.*

Figure 3.2: Bottom Layer.

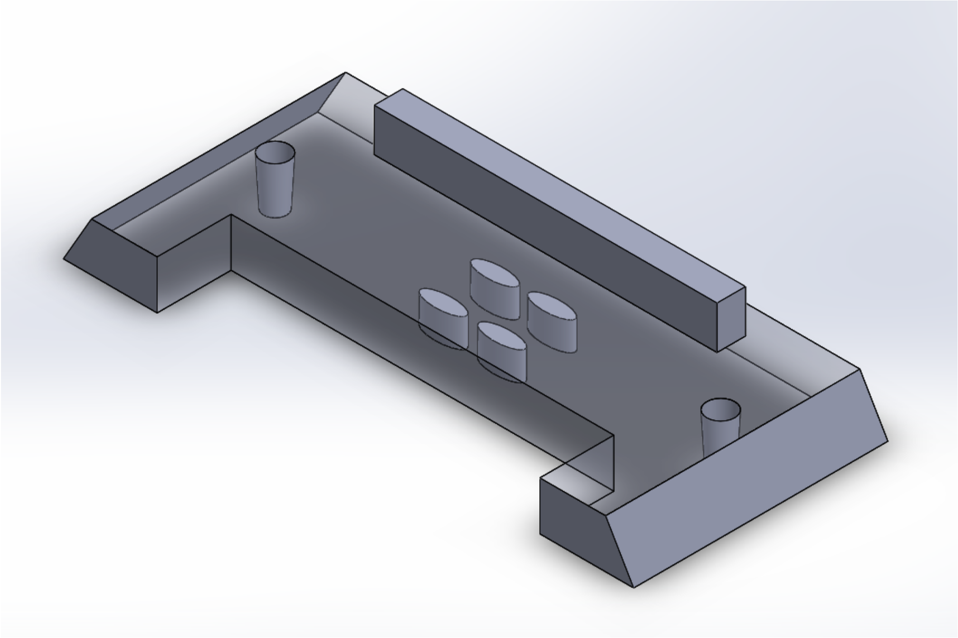

(a) *Isometric view.*

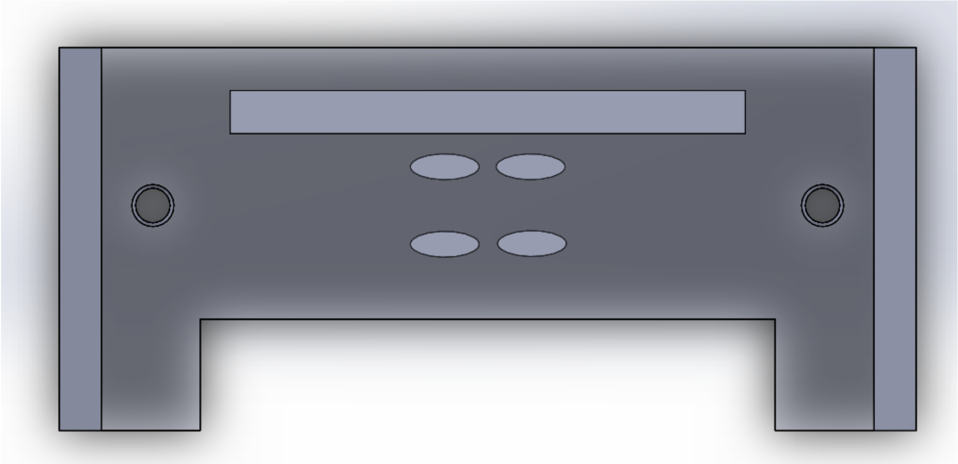

(b) *Top view.*

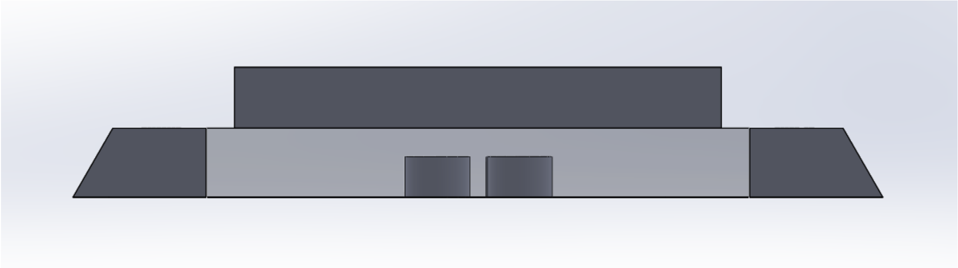

(c) *Front view.*

Figure 3.3: Top Layer.

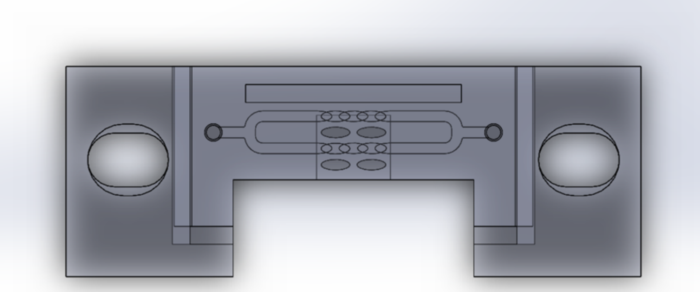

(a) First Configuration: loading step.

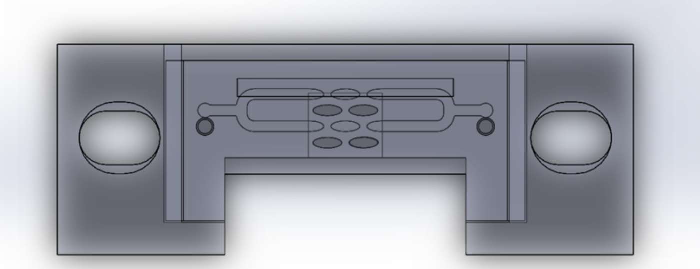

(b) Second Configuration: compartmentalisation step.

Figure 3.4: Loading and compartmentalisation process.

right where it has been illuminated by the UV laser. The printing proceeds automatically layer by layer until the object is complete.

The prototype was produced by ProtoLabs, a digital manufacturing company. The choice of the material was extremely challenging because numerous restrictions need to be considered at the same time:

- 3D-printability.
- Biocompatibility.
- Transparency.
- High temperature resistance.
- Proper wettability.

The biocompatibility is an essential requirement, since the DNA solution will be in touch with the material. So, neither the material itself nor its possible degradation products can cause the inhibition of the reaction. To control the success of the loading procedure an optical investigation is considered, and, for this reason, a clear material is preferable. During the LAMP reaction the temperature arises to 63° C, and then the material needs to withstand high temperature. Finally, in order to provide a loading with no leakage it is necessary to optimise the wettability of the surface.

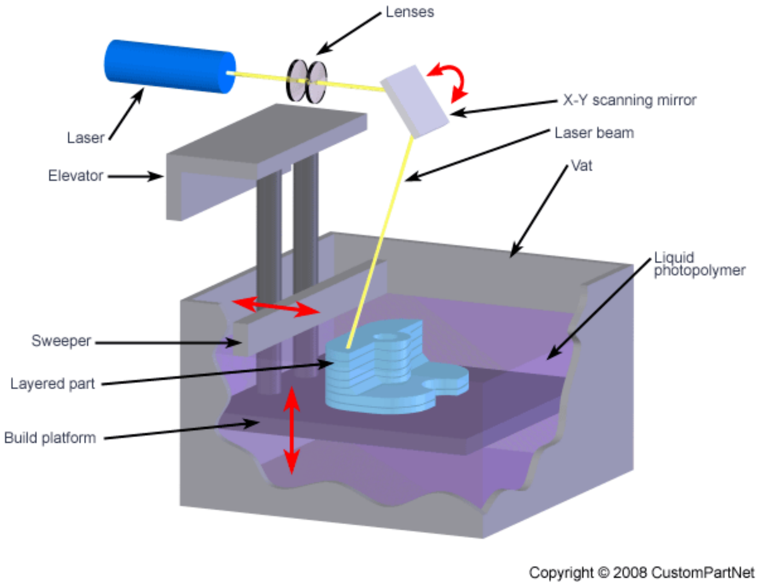

Figure 3.5: Schematic representation of Stereolithography. [11]

The material selected for the manufacturing is the Accura SL 5530, a transparent and polycarbonate-like resin. The characteristics of this material are listed in the Figure 3.6.

To increase the temperature resistance a thermal post-cure at 160°C was performed. In this way, the heat deflection temperature increases by around 100°C, ranging from 170°C to 250°C.

The Figure 3.7 illustrates the printed prototype.

3.3 Experimental Test

The microfluidic chip was first manually assembled under mineral oil. The bottom layer was placed inside a Petri dish filled by mineral oil. The top plate was then gently immersed avoiding the formation of bubbles, and placed on the top of the bottom plate. The two halves were later combined with two screws. The proper alignment between the two layers was checked by an optical investigation using a digital microscope. This step is also essential to control the absence of bubbles.

After the completely assembling of the chip, the experimental test continued with the loading of an aqueous solution. In the first trials a pH 4 buffer solution was considered, taking advantage of its pink colour. However, since the DNA sample solution has a certain viscosity, in the following trials a DNA-free reaction mix solution was specially prepared to this end and loaded in the chip. A green food colouring was also added to the solution

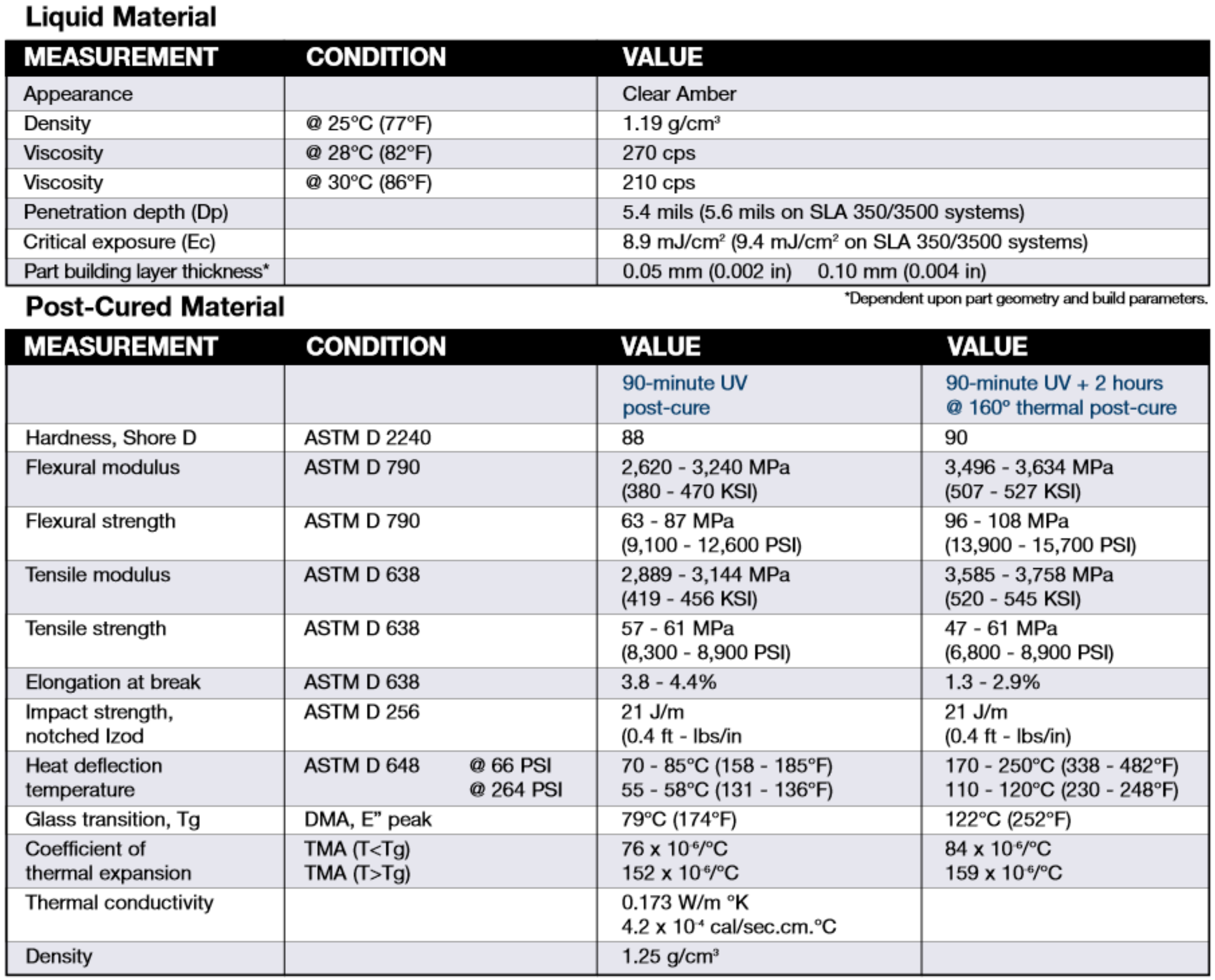

Liquid Material

MEASUREMENT	CONDITION	VALUE
Appearance		Clear Amber
Density	@ 25°C (77°F)	1.19 g/cm^3
Viscosity	@ 28°C (82°F)	270 cps
Viscosity	@ 30°C (86°F)	210 cps
Penetration depth (Dp)		5.4 mils (5.6 mils on SLA 350/3500 systems)
Critical exposure (Ec)		8.9 mJ/cm^2 (9.4 mJ/cm^2 on SLA 350/3500 systems)
Part building layer thickness*		0.05 mm (0.002 in) 0.10 mm (0.004 in)

*Dependent upon part geometry and build parameters.

Post-Cured Material

MEASUREMENT	CONDITION	VALUE	VALUE
		90-minute UV post-cure	90-minute UV + 2 hours @ 160° thermal post-cure
Hardness, Shore D	ASTM D 2240	88	90
Flexural modulus	ASTM D 790	2,620 - 3,240 MPa (380 - 470 KSI)	3,496 - 3,634 MPa (507 - 527 KSI)
Flexural strength	ASTM D 790	63 - 87 MPa (9,100 - 12,600 PSI)	96 - 108 MPa (13,900 - 15,700 PSI)
Tensile modulus	ASTM D 638	2,889 - 3,144 MPa (419 - 456 KSI)	3,585 - 3,758 MPa (520 - 545 KSI)
Tensile strength	ASTM D 638	57 - 61 MPa (8,300 - 8,900 PSI)	47 - 61 MPa (6,800 - 8,900 PSI)
Elongation at break	ASTM D 638	3.8 - 4.4%	1.3 - 2.9%
Impact strength, notched Izod	ASTM D 256	21 J/m (0.4 ft - lbs/in	21 J/m (0.4 ft - lbs/in)
Heat deflection temperature	ASTM D 648 @ 66 PSI @ 264 PSI	70 - 85°C (158 - 185°F) 55 - 58°C (131 - 136°F)	170 - 250°C (338 - 482°F) 110 - 120°C (230 - 248°F)
Glass transition, Tg	DMA, E" peak	79°C (174°F)	122°C (252°F)
Coefficient of thermal expansion	TMA (T<Tg) TMA (T>Tg)	76 x 10^{-6}/°C 152 x 10^{-6}/°C	84 x 10^{-6}/°C 159 x 10^{-6}/°C
Thermal conductivity		0.173 W/m °K 4.2 x 10^{-4} cal/sec.cm.°C	
Density		1.25 g/cm^3	

Figure 3.6: ACCURA SL 5530 material data sheet.

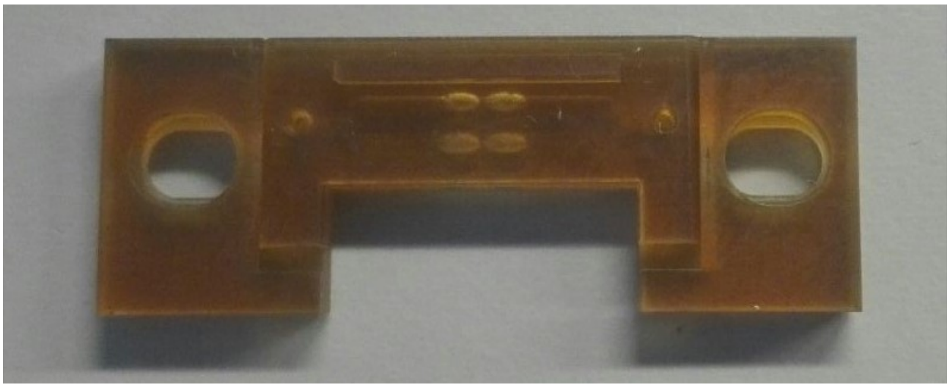

Figure 3.7: Picture of the 3D printed microfluidic chip.

to make it coloured and visible through the device.

The loading test was performed under the microscope by pipetting. A $10\mu l$ pipettor tip containing the solution was inserted in the inlet port of the chip. The solution was so dispensed inside the fluidic path and filled all the ducts and wells, replacing the oil. The surface tension should entail the solution to remain inside the channel and not spread around. Subsequently, the top plate was moved on the bottom plate into the second configuration. Once the top wells fully overlapped the chambers on the bottom, the solution should be able to fall down on the sensing array.

This experiment highlighted a number of issues during the operation of the microfluidic chip. Firstly, the sealing of the solution was not guaranteed, since it leaked inside the gap between the two plates. In particular, the spreading occurred at a certain period of time after the loading. This proves that the design of the channels and wells is correct and is not the cause of the leakage. Furthermore, after the "slipping", the solution was trapped inside the top wells and wasn't able to flow down and reach the microchip sensor. These problems prevent the employment of this microfluidic chip in the LoC platform, since it is not possible to perform a LAMP reaction in such a conditions where contamination can occur.

This may be due to the surface of the device is not completely smooth but is characterised by a certain degree of roughness. Moreover, the presence of spreading probably indicates that the ACCURA material is not hydrophobic enough so that the oil seals properly the solution inside the channel and wells.

Before proceeding with a following post-processing step aiming to a surface modification, it is however extremely important to assess a surface characterisation, estimating the roughness and the wettability to be the possible causes of the encountered problems.

Chapter 4

Surface characterisation

All surfaces are characterised by an higher energy state than bulk material and, for this reason, they can be easily subject to modification processes, resulting in a change of the surface energy.

In general, molecules of the same substance are bonded by intramolecular forces (such as Van der Waals forces or hydrogen bondings) that causes their cohesion. On the contrary, adhesive forces are attractive forces that can occur between molecules of different substance.

Given a system consisted by two different phases (1 and 2) separated by an interface, the atoms present in the bulk interact with atoms of the same species, resulting in a zero net force. The molecules present on the surface, instead, are less tightly bound since they are also surrounded by unlike molecules. As a result of these unbalanced forces, the net force is pointing inwards. These molecules are then characterised by a greater mobility and possess higher energy. The disruption of intermolecular bonds is the underlying reason which explains the generation of the *surface energy*, that can be thought of as the sum of all the excess energies of the surface atoms (see Figure 4.1).

It is possible to define the surface energy in term of the Gibbs free energy of the entire system (phase 1 plus phase 2 plus interface):

$$dG = -SdT + Vdp + \gamma_{12} dA \tag{4.1}$$

where γ_{12} is the *surface tension* and A is the area of the interface. Hence, γ_{12} is a force per unit length that equals the free Gibbs energy at constant pressure and temperature:

$$\gamma_{12} = \left(\frac{\partial G}{\partial A} \right)_{\text{constant T,p,n}} \tag{4.2}$$

As a result, the major reactivity of the molecules on the surface leads to spontaneous modification ($G < 0$) that decreases the surface area in order to minimise the surface energy state and achieve the thermodynamic stability.

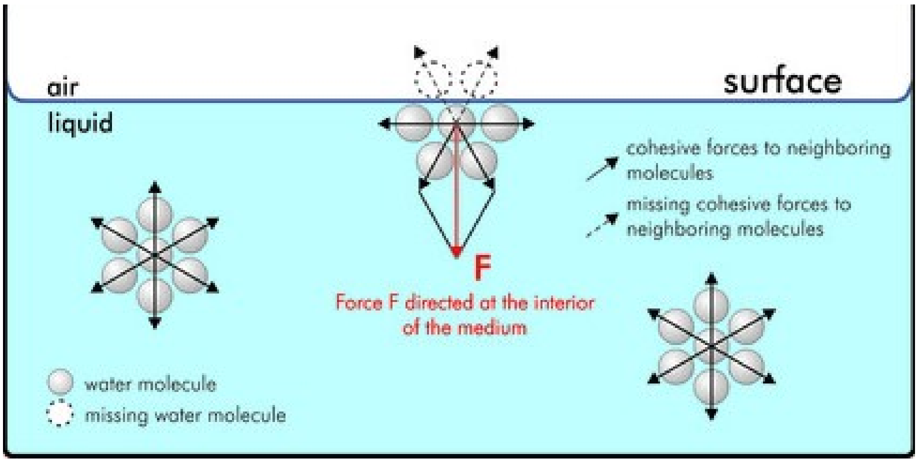

Figure 4.1: Surface Tension [12].

When a liquid comes into contact with a surface, both adhesive and cohesive forces play an important role in determining the shape of the interface. The effect of the surface tension between two different phases at equilibrium can be described by the Young-Laplace equation:

$$p_1 - p_2 = \gamma_{12}\left(\frac{1}{R_1} + \frac{1}{R_2}\right) \tag{4.3}$$

where R_1 and R_2 are the principal radii of curvature. This equation, which states that there is a pressure drop ($p_1 > p_2$) across the fluid interface, does not provide a direct method to calculate the surface tension since the measurement of the pressure difference and the radii of curvature could be difficult. Alternatively, it is possible to calculate the contact angle that measures the wettability of a solid surface by a liquid. In the design of any bio-device it is in fact extremely important to investigate the interaction of the device's surface with water. Considering a liquid droplet on an ideal surface (flat, rigid, perfectly smooth, and chemically homogeneous), there are three interfaces characterised by different surface tensions: γ_{SG} as the solid–vapor interfacial energy, γ_{SL} as the solid–liquid interfacial energy and γ_{LG} as the liquid–vapor interfacial energy. The contact angle θ_{c} is defined as the angle between the solid surface and the interface liquid-vapor.

At equilibrium, these three forces acting at the triple point (where all three phases coexist) sum to zero:

$$\gamma_{\mathrm{LG}} \cos\theta_{\mathrm{c}} + \gamma_{\mathrm{SL}} = \gamma_{\mathrm{SG}} \tag{4.4}$$

from which the following Young's equation derives:

$$\cos\theta_{\mathrm{c}} = \frac{\gamma_{\mathrm{SG}} - \gamma_{\mathrm{SL}}}{\gamma_{\mathrm{LG}}} \tag{4.5}$$

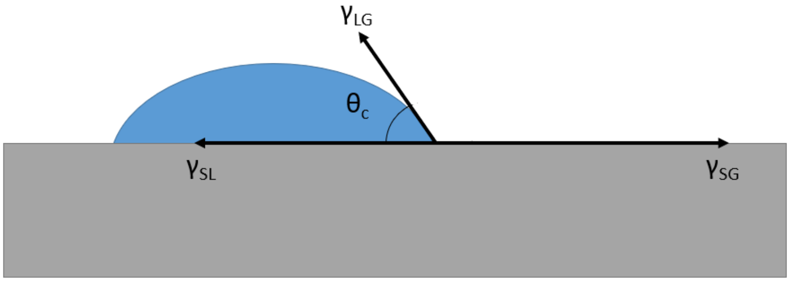

Figure 4.2: Contact Angle.

A surface is hydrophilic if it has the tendency to be wetted by water and this happens when $\theta_c < 90°$; otherwise, when the surface is repellent to water it is hydrophobic and exhibits a $\theta_c > 90°$. The sessile droplet method consists in the measurement of the contact angle through a contact angle goniometer, which allows the analysis of the profile of the droplet on the surface. There are many theoretical models that use contact angle data related to different liquid of known surface tension (probe liquid), to provide the surface energy of a solid substrate. Depending on which one is applied, a different value of surface energy is obtained. So, it is necessary to specify the methodology and the probe liquids used to have a meaningful surface energy measurement [3]. The Young's Equation (4.5) is applicable only in the case of an ideal surface. When a real surface is considered it is necessary to take into account the roughness. To this end, Wenzel introduced a new model described by the following equation:

$$\cos(\theta^{\star}_{\mathrm{W}}) = r\cos(\theta_{\mathrm{c}}) \tag{4.6}$$

where $\theta^{\star}_{\mathrm{W}}$ is the apparent contact angle, θ_c is the Young contact angle (relative to the corresponding ideal smooth surface) and r is the *roughness ratio* defined as the ratio between the contact area liquid-solid and the projected solid surface area ($r \geq 1$). Consequently, with the increase of roughness (higher r) the contact angle will increment, and so the surface will acquire a major hydrophobicity. When the rough surface is also chemical heterogeneous and is made of two components (1 and 2), the specific equation to be considered is the Cassie-Baxter's:

$$\cos(\theta^{\star}_{\mathrm{CB}}) = f_1\cos(\theta_1) + f_2\cos(\theta_2) \tag{4.7}$$

where the f_1 and f_2 represent the area fractions and θ_1 and θ_2 are the Young contact angles for the same surface but composed only by the component 1 and 2 respectively. The two models (see Figure 4.3) involve two different wetting processes: in the first one the drop permeates the surface and goes inside the grooves, instead in the second one the drop doesn't wet the surface completely but it is suspended on the top of the pillar surface.

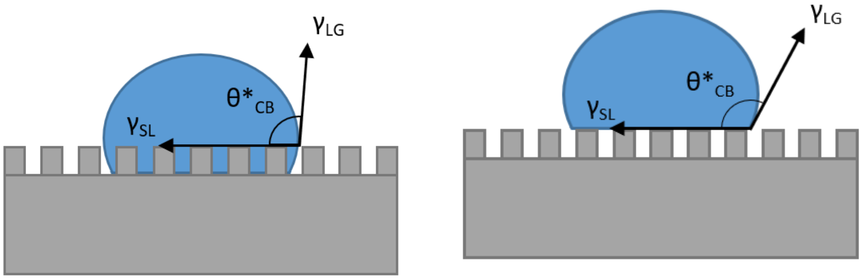

(a) *Wenzel model* (b) *Cassie-Baxter model*

Figure 4.3: Wetting models for a non ideal surface.

Sometimes after the deposition of a drop on the surface it is possible to assist to a transition from Cassie-Baxter's state to Wenzel's state. Sometimes the energy needed to step to one state to the other is provided by the kinetic energy during the deposition method. This results in the decrease of the measured contact angle. The transition is due to the release of the trapped air under the drop and its spreading in the grooves of the surface. Since the Cassie-Baxter is characterised by an higher energy level, this process is usually irreversible (the Cassie-Baxter represents a "metastable" equilibrium while the Wenzel state corresponds to a "stable" equilibrium) [33].

4.1 Owens and Wendt Theory [3]

The Owens and Wendt method allows to obtain the solid surface energy through measurements of the contact angle. This is considered a "two component" model for solid surface energy approach since it contemplates the surface energy of a solid substrate made of two components, the *dispersive component* and the *polar component*:

$$\gamma_S = \gamma_S^D + \gamma_S^P \tag{4.8}$$

$$\gamma_L = \gamma_L^D + \gamma_L^P \tag{4.9}$$

where γ_S is the overall surface energy of the solid and γ_L is the overall surface tension of the wetting fluid. The dispersive component is due to non-site specific interactions, such as van der Waals forces, and the polar component is instead due to site specific interactions, such as hydrogen bondings. The theory behind this method is based on the Young's Equation (4.5) and the Good's Equation:

$$\gamma_{SL} = \gamma_S + \gamma_L - 2\sqrt{\gamma_L^D \gamma_S^D} - 2\sqrt{\gamma_L^P \gamma_S^P} \tag{4.10}$$

From these equations, Owens and Wendt extract the following:

$$\frac{\gamma_L(\cos\theta+1)}{2\sqrt{\gamma_L^D}} = \sqrt{\gamma_S^P}\,\frac{\sqrt{\gamma_L^P}}{\sqrt{\gamma_L^D}} + \sqrt{\gamma_S^D} \tag{4.11}$$

A linear form $y{=}mx{+}b$ can be attributed to this equation, wherein:

$$y = \frac{\gamma_L(\cos\theta+1)}{2\sqrt{\gamma_L^D}} \tag{4.12}$$

$$m = \sqrt{\gamma_S^P} \tag{4.13}$$

$$x = \frac{\sqrt{\gamma_L^P}}{\sqrt{\gamma_L^D}} \tag{4.14}$$

$$b = \sqrt{\gamma_S^D} \tag{4.15}$$

Therefore, the γ_S of a surface can be determined by simply measuring the contact angle of two different liquids of known surface tension, called "probe liquids". With the plot of the linear function (4.11), from the intercept and the slope it is possible then to calculate the polar and dispersive components of the surface energy. However, to make this possible it is necessary to separate the overall surface tension of the probe liquid in the two component γ_L^D and γ_L^P. To do this, it is used a standard reference surface, usually in poly(tetrafluoroethylene) (PTFE), that has a surface energy of 18.0 mJ/m^2, and doesn't have polar interaction, so $\gamma_S = \gamma_S^D = 18.0\text{mJ/m}^2$. In this way, first the contact angle θ_{PTFE} is calculated for the two probe liquids, and then, for the Owens-Wendt equation (4.11), the dispersive component is obtained:

$$\gamma_L^D = \frac{\gamma_L^2(\cos\theta_{PTFE}+1)^2}{72} \tag{4.16}$$

and as a consequence, also the polar component $\gamma_L^P = \gamma_L - \gamma L^P$. In the end, once the γ_L^D and γ_L^P of the two probe liquids are known, it is possible to apply the Owens-Wendt model to obtain the γ_S of the surface.

4.2 Spreading Parameter [4]

Another important parameter to evaluate the wettability of the surface is the *Spreading Parameter* defined as the difference between the work of adhesion W_a and the work of cohesion W_c:

$$S = W_a - W_c \tag{4.17}$$

The W_a can be described in terms of surface energies γ. Given two phases α and β in contact in equilibrium separated by an interface, the work of adhesion is the work needed to cleave the two phases in a third phase ω (see Figure 4.4).

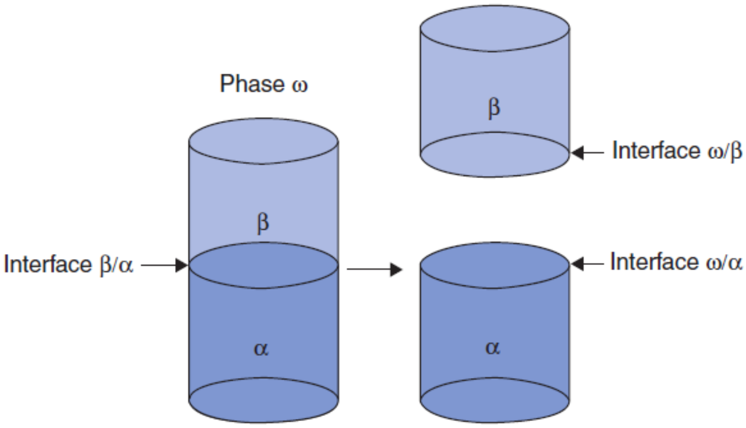

Figure 4.4: Work of adhesion [13].

$$W_{\alpha\beta} = \gamma_{\alpha\omega} + \gamma_{\beta\omega} - \gamma_{\alpha\beta} \tag{4.18}$$

Then, when a surface wetted by a liquid in equilibrium is considered, the W_a can be obtained by the Young-Dupré's equation:

$$W_a = \gamma_S + \gamma_L - \gamma_{SL} \tag{4.19}$$

where γ_S is the overall surface energy of the substrate, the γ_L is the overall surface energy of the liquid and the γ_{SL} is the interfacial energy between the solid and the liquid. Combining this equation with the Young's one (4.5):

$$W_a = \gamma_L(1 + \cos\theta_C) \tag{4.20}$$

It is possible to think of the work of cohesion W_c as a particular case of W_a in which the two phases are the same. Relatively to a fluid wetting a surface:

$$W_c = 2\gamma_L \tag{4.21}$$

Thus:

$$S = \gamma_S - (\gamma_{SL} + \gamma_L) \tag{4.22}$$

Taking also into account the two components model for the surface energy (4.8 and 4.9), the spreading parameter becomes:

$$S = 2\left(\sqrt{\gamma_L^D \gamma_S^D} + \sqrt{\gamma_L^P \gamma_S^P} - \gamma_L\right) \tag{4.23}$$

Probe liquids	**Total Surface tension** γ (mN/m)	**Dispersive component** γ^D (mN/m)	**Polar component** γ^P (mN/m)
Water	72.80	21.80	51.00
Diodomethane	50.80	50.80	0

Table 4.1: Surface tension and its components for probe liquids (adapted from [4]).

4.3 Experimental Data

For the measurement of the surface energy of the manifold the two probe liquids used were demineralised water and diiodomethane (also known as methylene iodide, MI), of which the dispersive and polar components were previously obtained using a PTFE surface as a standard reference [4] (see Table 4.1).

Prior to the measurement of the contact angle, the manifolds were cleaned with high-purity ethanol in order to remove any possible contamination, then wiped with a cloth and dried in a stream of hot air. The contact angle was measured with the static sessile drop method using an advanced automated contact angle goniometer (*ramé-hart* contact angle goniometer, Model 590) (see Figure 4.5). The equipment consists of an horizontal optical bench to place the solid sample, an automated dispensing system and a microsyringe to form the liquid droplet, an illuminator and fiber optic bundle, a digital camera and a DROPimage Advanced Software [14]. The contact angle is

Figure 4.5: A *ramé-hart* contact angle goniometer [14].

obtained considering the profile of a sessile droplet and calculating the slope of the tangent to the drop at the three-phase point. This method of drop shape analysis is based on two hypothesis [34]:

- The drop is symmetric with a central vertical axis.
- The only forces influencing the drop shape are the interfacial tension and gravity.

At the beginning it was necessary to setup the instrument, adjusting the lightning and the camera focusing and magnification. The test fluids, water and the diiodiomethane, were placed in the syringe. Given the drop volume of 5μl, the pump was then calibrated on the basis of the syringe internal diameter. Since the diiodiomethane is more viscous than water [35], the pumping rate was optimised in order to compensate the higher pressure drop across needle. The measurements were performed on the two internal surfaces of the manifold (the bottom side for the top layer and the top side for the bottom layer). To have a reliable measurement the drop needs to be dispensed reducing the kinetic energy as much as possible, since it would cause its spreading. An attempt to solve this problem is to accomplish the dispensation forming a pendant drop and then moving the sample closer to the bottom of the drop, so that the adhesion involves the detachment of the drop from the needle. Once the drop was deposited on the surface, the image analysis software was calibrated to set-up the baseline needed for the measurement. It was selected the horizontal liquid-solid interface. Since this

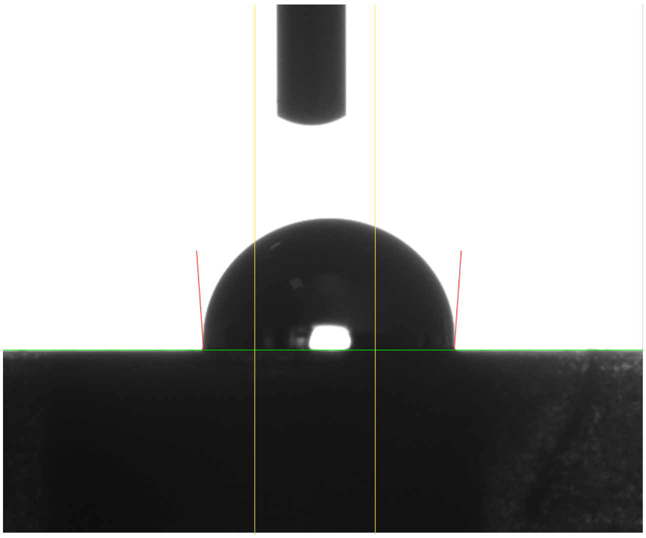

Figure 4.6: Automated calculation of the right and left contact angles by the DROPimage Advanced Software. In red the tangents to the drop on the two sides, and in green the baseline.

was a manual procedure an average error of ±1° was applied to the obtained contact angle data. The software is able to calculate the right and the left contact angle, θ_{C_R} and θ_{C_S}, for each time-frame (see Figure 4.6). The contact angle θ_C reported is simply the mean value of these two. The calculation is carried on for a certain amount of time-frame to assess if the measurement is stable or undergoes gradual decreasing. Since the time interval between two consecutive time steps is always of 0.02 seconds, it was then possible to convert the data set in time. Each contact angle calculation was repeated three times and a statistical evaluation was subsequently performed in order to provide an average value. For the bottom layer, the Figure 4.7 shows the average values for the θ_{C_R}, θ_{C_S} and the θ_C when a 5μl drop of water is deposited on the surface of the bottom layer. The starting values should not be considered in the evaluation of the contact angle, since the drop was unstable immediately after the deposition procedure. Indeed, the contact angles decreased in time, and this clearly shows that the measurement was not static but dynamic. This probably indicates a spreading of the liquid drop on the surface because of its roughness. The theory underneath this process is explained by the Cassie–Baxter to Wenzel transition. In order to extrapolate a contact angle representative of the surface only the values related to time steps from 20 to 100 (0.4s to 2s) were considered. The contact angle θ_{C_W} is around 98.6°±1°.

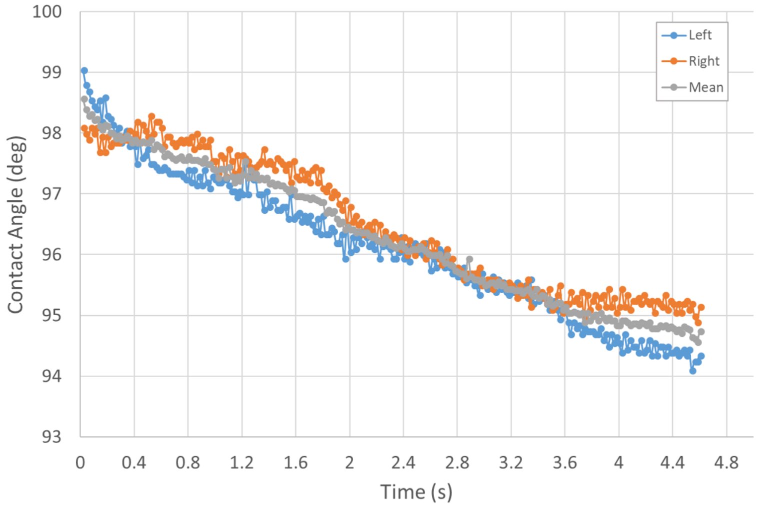

Figure 4.7: Contact angle of 5μl water drop on the bottom layer.

The experimental measurement was then repeated with a MI drop. In this case (see Figure 4.8) the measurement was stable in time and the $\theta_{C_{MI}}$ plateaued at value little less than 65°.

The same test was subsequently done for the top layer of the manifold, in order to control potential changes in the surface of the two pieces during

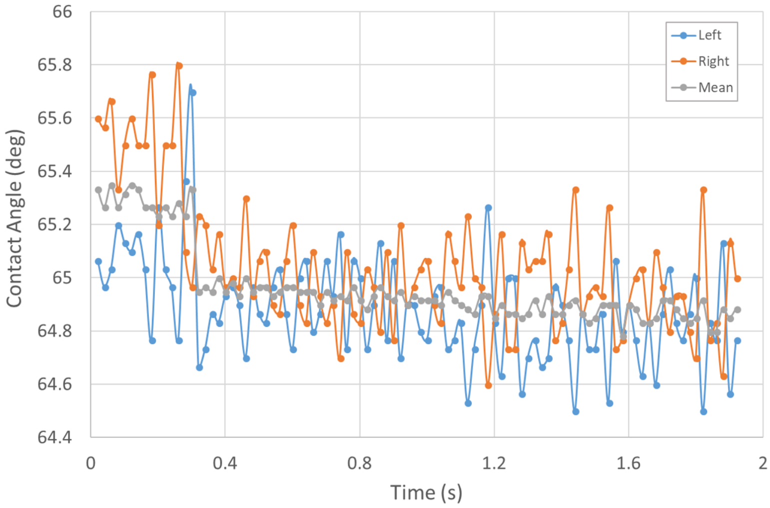

Figure 4.8: Contact angle of 5μl MI drop on the bottom layer.

the manufacturing process. With water as probe liquid (see Figure 4.9), the contact angle θ_{C_W} is around 76.5°±1°. There is then a considerable difference in the wettability characterising the two layers. For the MI drop, the Figure 4.10 illustrates that the contact angle $\theta_{C_{MI}}$ was extremely stable at value of 69.3°, similar to the one obtained for the bottom layer.

The images *a*-*c* (see Figure 4.11) taken by the digital camera of the goniometer during the test clearly show that the top layer is more hydrophilic than the bottom layer, as the drop of water is less round on the surface.

The surface energy was later calculated according to the Owens-Wendt method. The linear function was plotted both for the two layers (see Figure 4.12). For the bottom layer the dispersive component γ_S^D obtained from the intercept is of $0.52 mJ/m^2$, while the polar component γ_S^P obtained from the slope is of $25.70 mJ/m^2$, resulting in an overall surface energy γ_S of $26.22 mJ/m^2$. For the top layer instead the γ_S^P is of $8.72 mJ/m^2$, γ_S^D is of $23.27 mJ/m^2$, and the overall surface energy γ_S is $31.98 mJ/m^2$.

In the end the spreading parameter S was measured according to the 4.23. For the bottom layer S was of -83.79, and for the top was of -55.81. The negative values indicate that a partial wetting occurred since the work of the cohesion of the water was higher than the work of adhesion.

The same measurements should then be repeated after a surface modification process in order to compare the weattability of the manifold's surface, and to control if the process was accomplished successfully.

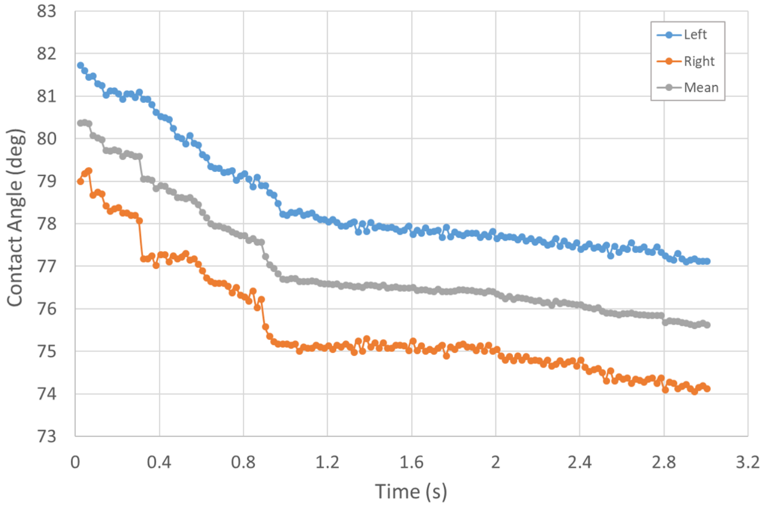

Figure 4.9: Contact angle of 5μl water drop on the top layer.

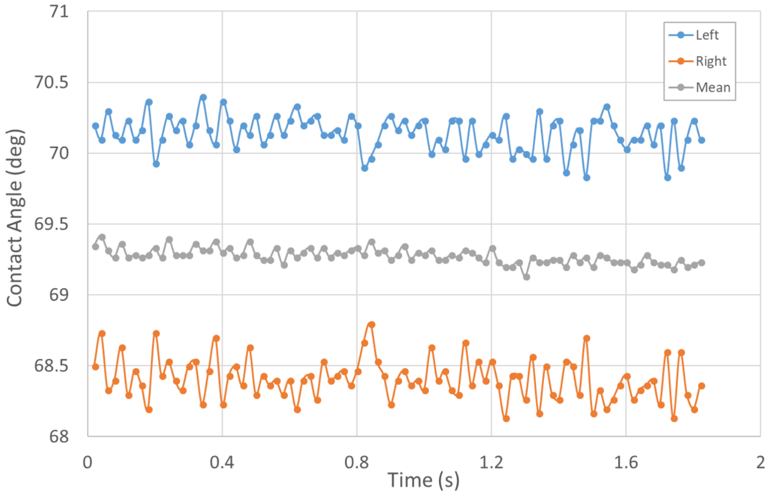

Figure 4.10: Contact angle of 5μl MI drop on the top layer.

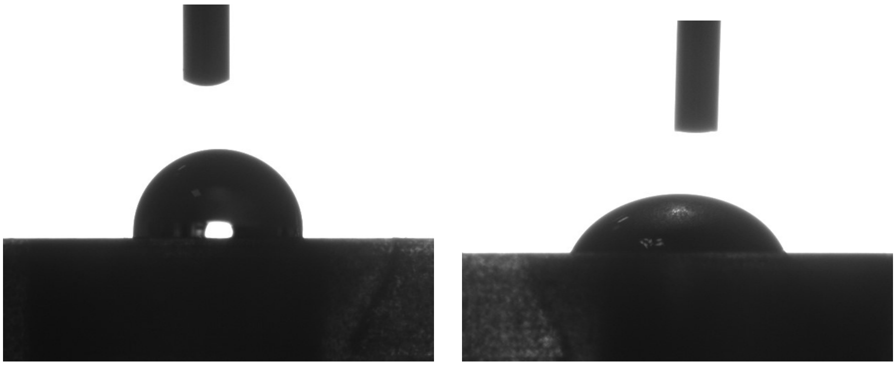

(a) *5μl water drop on the bottom layer* (b) *5μl MI drop on the bottom layer*

(c) *5μl water drop on the top layer* (d) *5μl MI drop on the top layer*

Figure 4.11: Contact angles images.

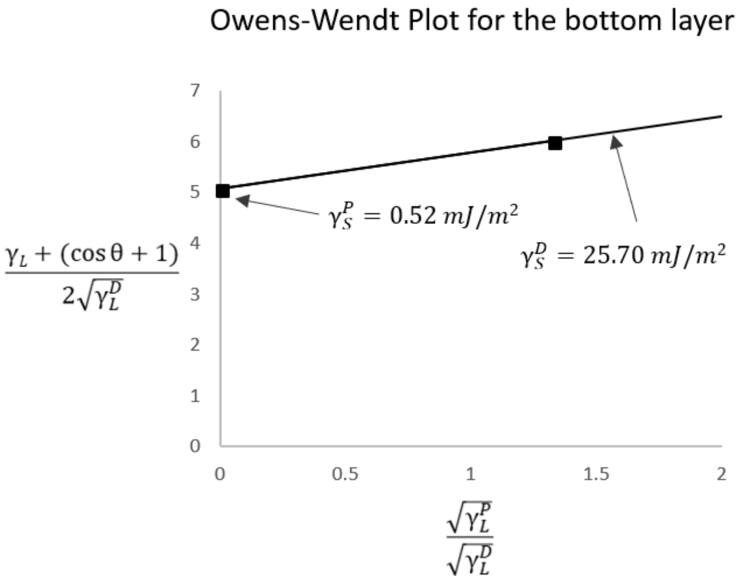

(a) *Plot for the bottom layer*

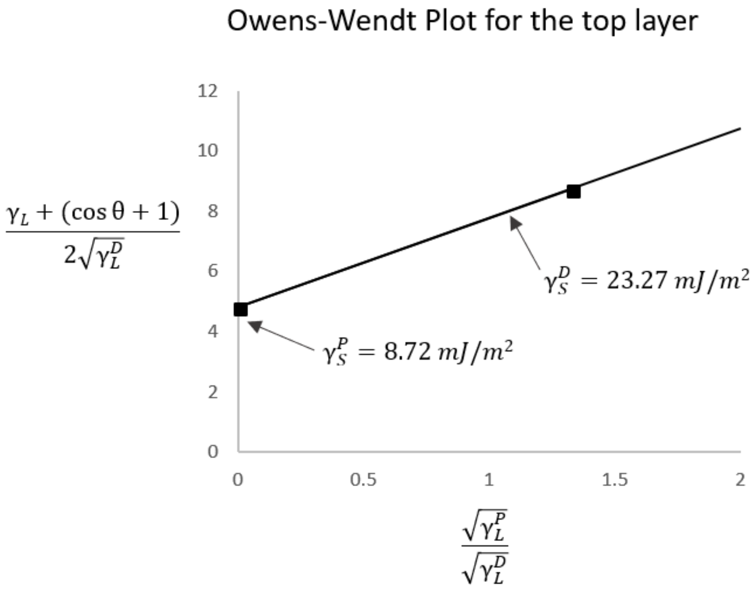

(b) *Plot for the top layer*

Figure 4.12: Owens-Wendt surface energy calculation plot.

Chapter 5

Conclusions

The focus of this thesis was the design of a microfluidic device to be incorporated with a microchip sensor able to detect ion-activity during DNA amplification, and used for early diagnosis of infectious diseases. The work has been carried out during a nine month exchange project at the "Centre for Bio-Inspired Technology", Imperial College London (UK).

As planned, a prototype of such a microfluidic device has been assembled. Also, obstacles and limitations that arise when testing this type of device have been evaluated.

The initial state-of-the-art analysis highlighted the prevalent approaches currently adopted and their limitations. The demand for reduced-cost, rapid, portable and high-sensitive tests led to the development of the LoC technology.

In the prototyping stage, a microfluidic device has been realised by 3D printing to compartmentalise the solution in four separated chambers. Multiple issues have been raised in the prototype implementation. Firstly, the leakage of the solution between the two plates of the manifold prevents a proper isolation of the solution in the reaction chambers. This makes impossible the performance of the DNA amplification reaction, since a DNA-contamination is extremely likely. Secondly, the solution is not able to get in touch with the sensors, since it remains trapped in the microfluidic wells of the top plate.

In order to elucidate the limitations encountered, a surface characterisation was attempted. The analysis of the results showed the surfaces were not hydrophobic enough to have a sealing of the solution by the oil phase.

5.1 Future work

After the realisation of this first prototype of the microfluidic device, important work has to be done in the future.

The immediately following step may be the implementation of a post-processing by enhancing the hydrophobicity of the surface of the manifold. Moreover, another step could also be the employment of a 3D printer characterised by a better resolution, so that the features of the device can be realised with an higher accuracy.

Once the prototype is fully functional, an alternative to a 3D printing process needs to be considered, in order that the production could be established on a large scale.

Lastly, the ultimate goal of this project may be the integration of the sample processing to achieve a completely portable and automatic device.

Bibliography

[1] T. Notomi, H. Okayama, H. Masubuchi, T. Yonekawa, K. Watanabe, N. Amino, and T. Hase, "Loop-mediated isothermal amplification of DNA.," *Nucleic acids research*, vol. 28, no. 12, p. E63, 2000.

[2] N. Moser, J. Rodriguez-Manzano, T. S. Lande, and P. Georgiou, "A scalable ISFET sensing and memory array with sensor auto-calibration for on-chip real-time DNA detection," *IEEE Transactions on Biomedical Circuits and Systems*, vol. 12, no. 2, pp. 390–401, 2018.

[3] K. GmbH, "Measure Surface Energy: A tutorial designed to provide basic understanding of the concept of solid surface energy," *Kruss*, pp. 1–8, 1999.

[4] M. Kalin and M. Polajnar, "The correlation between the surface energy, the contact angle and the spreading parameter, and their relevance for the wetting behaviour of DLC with lubricating oils," *Tribology International*, vol. 66, pp. 225–233, 2013.

[5] WHO, "The top 10 causes of death," 2018.

[6] "PCR Cycling Parameters—Six Key Considerations for Success - UK,"

[7] M. W. Pfaffl, *MIQE & qPCR ibook how to apply the MIQE guidelines - a visual, interactive and practical qPCR guide!* bioMCC, 2015.

[8] M. G. Mauk, J. Song, C. Liu, and H. H. Bau, "Simple approaches to minimally-instrumented, microfluidic-based point-of-care Nucleic Acid Amplification Tests," *Biosensors*, vol. 8, no. 1, 2018.

[9] W. Du, L. Li, K. P. Nichols, and R. F. Ismagilov, "SlipChip," *Lab on a Chip*, vol. 9, no. 16, pp. 2286–2292, 2009.

[10] S. Haeberle, D. Mark, F. Von Stetten, and R. Zengerle, "Microfluidic platforms for lab-on-a-chip applications," *Microsystems and Nanotechnology*, vol. 9783642182, no. 9, pp. 853–895, 2012.

[11] ZARE, "Stereolitografia (SLA): tecnica consolidata per un dettaglio elevato."

[12] SITA, "Process parameter surface tension."

[13] Kino, "Work of adhesion and Young-Laplace equation–Theory of surface tension, contact angle, wetting and work of adhesion (4)_USA KINO Industry Co., Ltd.."

[14] Ramé-Hart, "ramé-hart Goniometer/Tensiometer Model 590."

[15] O'Neill J., "Tackling drug-resistant infections globally: fi nal report and recommendations. The review on antimicrobial resistance.," no. May, 2016.

[16] XXPRESS, "What are the phases of PCR amplification? - xxpresspcr."

[17] Eiken, "The principle of LAMP method."

[18] P. Tabeling, *Introduction to Microfluidics.* Oxford University Press, 2005.

[19] S. S. Saliterman, *Fundamentals of BioMEMS and Medical Microdevices.* SPIE PRESS, 2006.

[20] M. B. Xiwei Zheng, Cong Bi and D. S. Hage, "HHS Public Access," *Anal Chem.*, vol. 25, no. 4, pp. 368–379, 2015.

[21] luxresearch, "Health Care Microfluidics Market to Grow to Nearly $4 Billion in 2020 | Lux Research."

[22] Y. Fu, H. Zhou, C. Jia, F. Jing, Q. Jin, J. Zhao, and G. Li, "A microfluidic chip based on surfactant-doped polydimethylsiloxane (PDMS) in a sandwich configuration for low-cost and robust digital PCR," *Sensors and Actuators, B: Chemical*, vol. 245, pp. 414–422, 2017.

[23] A. M. Thompson, A. Gansen, A. L. Paguirigan, J. E. Kreutz, J. P. Radich, and D. T. Chiu, "Self-digitization microfluidic chip for absolute quantification of mRNA in single cells," *Analytical Chemistry*, vol. 86, no. 24, pp. 12308–12314, 2014.

[24] A. Yamada, F. Barbaud, L. Cinque, L. Wang, Q. Zeng, Y. Chen, and D. Baigl, "Oil microsealing: A robust micro-compartmentalization method for on-chip chemical and biological assays," *Small*, vol. 6, no. 19, pp. 2169–2175, 2010.

[25] S. Begolo, D. V. Zhukov, D. A. Selck, L. Li, and R. F. Ismagilov, "The pumping lid: Investigating multi-material 3D printing for equipment-free, programmable generation of positive and negative pressures for microfluidic applications," *Lab on a Chip*, vol. 14, no. 24, pp. 4616–4628, 2014.

[26] ILLUMINA, "Digital Microfluidics Technology."

[27] J. Gong and C. J. Kim, "All-electronic droplet generation on-chip with real-time feedback control for EWOD digital microfluidics," *Lab on a Chip*, vol. 8, no. 6, pp. 898–906, 2008.

[28] K. Khoshmanesh, S. Nahavandi, S. Baratchi, A. Mitchell, and K. Kalantar-zadeh, "Dielectrophoretic platforms for bio-microfluidic systems," *Biosensors and Bioelectronics*, vol. 26, no. 5, pp. 1800–1814, 2011.

[29] M. C. Morales, H. Lin, and J. D. Zahn, "Continuous microfluidic DNA and protein trapping and concentration by balancing transverse electrokinetic forces," *Lab on a Chip*, vol. 12, no. 1, pp. 99–108, 2012.

[30] P. Georgiou and C. Toumazou, "ISFET characteristics in CMOS and their application to weak inversion operation," *Sensors and Actuators, B: Chemical*, vol. 143, no. 1, pp. 211–217, 2009.

[31] DNA Electronics, "LiDia," 2018.

[32] A. Au, N. Moser, J. Rodriguez-manzano, and P. Georgiou, "Live Demonstration : A Mobile Diagnostic System for Rapid Detection and Tracking of Infectious Diseases," vol. 17, no. 99, p. 5386, 2018.

[33] B. J. Kirby, *Micro- and Nanoscale Fluid Mechanics: Transport in Microfluidic Devices.* Cambridge University Press, 2010.

[34] R. Woodward, "Contact angle measurements using the drop shape method," *First Ten Angstroms Inc., Portsmouth, VA*, vol. 66, no. Lvl, pp. 1–8, 1999.

[35] DIVERSIFIED-Enterprises, "Viscosity, Surface Tension, Specific Density and Molecular Weight of Selected Liquids."